Chapter 8

Design of Galerkin/Least-Squares Methods in the Frequency Domain

As discussed in the introduction to this thesis, for linear problems characterized by a relatively small range of frequencies, a time-dependent solution to the structural acoustics problem may be obtained indirectly in the frequency domain through a Fourier transform. The Fourier transform $\tilde{f}(\boldsymbol{x}\,,\,\omega)$ of a function $f(\boldsymbol{x}\,,\,t)$ is defined as,

$$\tilde{f}(\boldsymbol{x}\,,\,\omega) := \frac{1}{\sqrt{2\pi}} \int_{-\infty}^{\infty} f(\boldsymbol{x}\,,\,t) e^{i\omega t}\, dt \tag{8.1}$$

where ω is the temporal transform parameter or circular frequency and $i = \sqrt{-1}$. Application of the Fourier transform to the differential equations (2.27) - (2.33) governing structural acoustics leads to the strong (local) form of the boundary value problem in the frequency-domain.

Strong Form of the Time-Harmonic Problem

For a given frequency $\omega > 0$,
Find the displacement vector $\boldsymbol{u}(\boldsymbol{x}\,,\,\omega) : \bar{\Omega}_s \mapsto \mathbb{C}^d$, and the acoustic velocity potential $\phi(\boldsymbol{x}\,,\,\omega) : \bar{\Omega}_f \mapsto \mathbb{C}$, such that the following differential equations are satisfied:

$$\nabla \cdot \boldsymbol{\sigma} + \rho_s \omega^2 \boldsymbol{u} = \boldsymbol{0} \qquad \text{in } \Omega_s \tag{8.2}$$

$$\boldsymbol{\sigma} = \boldsymbol{C} : \nabla^s \boldsymbol{u} \qquad \text{in } \Omega_s \tag{8.3}$$

$$\nabla^2\phi + k^2\phi = f \qquad \text{in } \Omega_f \tag{8.4}$$

$$\boldsymbol{\sigma}\cdot\boldsymbol{n} = \bar{\boldsymbol{t}} \qquad \text{on } \Gamma_\sigma \tag{8.5}$$

$$\boldsymbol{\sigma}\cdot\boldsymbol{n} = -i\omega\rho_0\phi\boldsymbol{n} \qquad \text{on } \Gamma_i \tag{8.6}$$

$$\nabla\phi\cdot\boldsymbol{n} = -i\omega\boldsymbol{u}\cdot\boldsymbol{n} \qquad \text{on } \Gamma_i \tag{8.7}$$

$$\nabla\phi\cdot\boldsymbol{n} = -\mathbb{S}_m\phi \qquad \text{on } \Gamma_\infty \tag{8.8}$$

In the above, $k = \omega/c$, is the acoustic wavenumber where c is the speed of sound in the fluid medium. The acoustic pressure is calculated simply as $p = i\omega\rho_0\phi$. Equation (8.8) is either a local or nonlocal non-reflecting boundary condition defined through the operator $\mathbb{S}_m$. An alternative is to replace the boundary condition (8.8) with an infinite element, see BURNETT [1993].

Time-harmonic acoustic radiation and scattering from complex structures such as submarines can be predicted accurately at the lower and higher ends of the frequency spectrum using existing solution techniques. At high frequencies characterized by normalized frequencies above $ka > 20$, where a is a length scale associated with the geometry, e.g. for an end-capped cylinder, the scale a measures the radius of the cylinder, approximate ray methods based on the geometrical theory of diffraction KELLER [1962], can be used effectively. At low frequencies $ka < 10$, standard numerical methods such as the Galerkin finite element method, see for example ZIENKIEWICZ AND BETTESS [1978], are effective for obtaining accurate solutions. However, as the frequency increases for a fixed mesh size, finite element solutions using the standard Galerkin approach deteriorate in accuracy. A standard rule of thumb is that ten linear elements are needed to accurately resolve a single wavelength. While there is no intrinsic limit on the size of frequency that can be handled using standard finite element methods, i.e. the mesh can always be refined to maintain a specified resolution accuracy; for large frequencies above $ka > 10$, the modeling effort required to satisfy this criteria can be prohibitive. Thus for high frequencies the number of degrees of freedom in a Galerkin finite element model can be overwhelming. A remark here is that the normalized frequency limits stated are only estimates, and may vary somewhat depending on the complexity of the structure and loading.

In this Chapter a simple enhancement of the standard Galerkin method, referred to as the Galerkin/Least-Squares (GLS) method is developed to address the problem of obtaining increased accuracy with a minimum number of degrees of freedom; in effect extending the range of the finite element solutions to higher frequency calculations. The starting point is the equivalent weak form of the time-harmonic boundary value problem defined in (8.2) through (8.8). The weak form can be obtained through a weighted residual statement and integration by parts.

Weak Form of the Time-Harmonic Problem

For a given frequency $\omega > 0$,
Find $(\boldsymbol{u}\, ,\, \phi) \in \mathcal{S} \times \mathcal{T}$, such that $\forall\, (\boldsymbol{w}\, ,\, w) \in \mathcal{V} \times \mathcal{W}$,

$$G_s(\boldsymbol{w}\, ,\, \boldsymbol{u}) + i\omega A(\boldsymbol{w}\, ,\, \phi)_{\Gamma_i} \;=\; F_s(\boldsymbol{w}) \tag{8.9}$$

$$G_f(w\, ,\, \phi) - i\omega A(w\, ,\, \boldsymbol{u})_{\Gamma_i} \;=\; F_f(w) \tag{8.10}$$

where the sesquilinear operators for the structure and fluid are respectively,

$$G_s(\boldsymbol{w}\, ,\, \boldsymbol{u}) \;:=\; a_s(\boldsymbol{w}, \boldsymbol{u}) - \omega^2(\boldsymbol{w}, \boldsymbol{u}) \tag{8.11}$$

$$G_f(w\, ,\, \phi) \;:=\; a_f(w, \phi) - k^2(w, \phi) + (w\, ,\, \mathbb{S}_m\phi)_{\Gamma_\infty} \tag{8.12}$$

with

$$(\boldsymbol{w}, \boldsymbol{u}) \;=\; \int_{\Omega_s} \rho_s\, \boldsymbol{w} \cdot \boldsymbol{u}\; d\Omega \tag{8.13}$$

$$a_s(\boldsymbol{w}, \boldsymbol{u}) \;=\; \int_{\Omega_s} \nabla\boldsymbol{w} : \boldsymbol{C} : \nabla\boldsymbol{u}\; d\Omega \tag{8.14}$$

$$a_f(w, \phi) \;=\; \int_{\Omega_f} \rho_0\, \nabla w \cdot \nabla\phi\; d\Omega \tag{8.15}$$

$$(w, \phi) \;=\; \int_{\Omega_f} \rho_0\, w\, \phi\; d\Omega \tag{8.16}$$

$$A(\boldsymbol{w}\, ,\, \phi)_{\Gamma_i} \;=\; \int_{\Gamma_i} \rho_0\, \boldsymbol{w} \cdot \boldsymbol{n}\phi\; d\Gamma \tag{8.17}$$

$$A(w\, ,\, \boldsymbol{u})_{\Gamma_i} \;=\; \int_{\Gamma_i} \rho_0\, w\, \boldsymbol{u} \cdot \boldsymbol{n}\; d\Gamma \tag{8.18}$$

$$F_s(\boldsymbol{w}) = \int_{\Gamma_\sigma} \boldsymbol{w} \cdot \bar{\boldsymbol{t}} \, d\Gamma \tag{8.19}$$

$$F_f(w) = \int_{\Omega_f} \rho_0 \, w \, f \, d\Omega \tag{8.20}$$

$$(w \,,\, \mathbb{S}_m \phi)_{\Gamma_\infty} = \int_{\Gamma_\infty} \rho_0 \, w \, \mathbb{S}_m \, \phi \, d\Gamma \tag{8.21}$$

and where the trial and weighting function spaces are defined as,

$$\mathcal{S} = \mathcal{V} = \left\{ \boldsymbol{u} | \boldsymbol{u} : \Omega_s \mapsto \mathbb{C}^d, \boldsymbol{u} \in (H^1(\Omega_s))^d \right\} \tag{8.22}$$

$$\mathcal{T} = \mathcal{W} = \left\{ \phi | \phi : \Omega_f \mapsto \mathbb{C}, \phi \in H^1(\Omega_f) \right\} \tag{8.23}$$

Note that this weak form can also be obtained directly from the Fourier transform of the variational equation given in Chapter 7 for the semidiscrete formulation. The Galerkin finite element method is obtained by partitioning the domain into finite elements and by introducing discrete approximations to the trial and weighting functions. After solving for the time-harmonic displacements and acoustic pressures, the time-dependent solution can then be obtained indirectly by a Fast Fourier Transform (FFT) inversion algorithm of the frequency-domain solution. Of course if the dynamic disturbance varies harmonically with time as $\mathrm{e}^{-i\omega t}$, i.e. the steady-state problem, or the analyist is only interested in the time-harmonic frequency response, then no such inversion is necessary.

In the Galerkin/Least-Squares (GLS) method, additional terms involving residuals of the governing differential equations are added to the Galerkin variational equation in least-squares form. In this thesis the design of GLS finite element methods for the Helmholtz equation governing the acoustic fluid medium are considered. The ideas presented here can also be extended to the structural response, but will not be addressed here. Applications to one-dimensional structural elements can be found in Grosh and Pinsky [1993b].

8.1 Background

Finite element solutions to the Helmholtz equation have primarily been sought using the standard Galerkin method; for applications see for example, MacCamy and

Marin [1980], Goldstein [1982], Bayliss, Goldstein and Turkel [1985a] and Burnett [1993]. However, it is well known that the numerical phase accuracy of standard Galerkin finite element solutions deteriorate rapidly as the wavenumber, normalized with the element mesh size, is increased, Belytschko and Mullen [1978], Mullen and Belytschko [1982]. This resolution problem arises from the use of piecewise polynomial shape functions to approximate highly oscillatory wave propagation solutions. To obtain an acceptable level of accuracy, more than ten elements per wavelength are required and for large wavenumbers, refining the mesh to maintain this requirement may become prohibitively expensive. Global error estimates for the Galerkin finite element method in terms of the wavenumber and local element size are derived in Bayliss, Goldstein and Turkel [1985b], Aziz, Kellogg and Stephens [1988] and Douglas, Santos, Sheen, and Schreiyer [1993].

Several approaches designed to improve the numerical phase accuracy of the standard Galerkin method have been proposed in recent years. Goldstein [1986] employed a version of the weak element method to the Helmholtz equation where the local solution within each element is approximated by a sum of exponentials. In this approach, continuity at interelement boundaries is enforced weakly for certain functionals of the approximate solution. As reported by Goldstein, for general problems in two-dimensions, the success of this approach has been limited.

Park and Jensen [1989] and Alvin and Park [1991] used discrete Fourier analysis to derive wavenumber dependent modifications to the stiffness and mass matrices arising from standard Galerkin finite element methods. The modified element matrices are designed to minimize dispersion error over a specified frequency–wavenumber window. This approach can be viewed as an extension of previous modifications to Galerkin finite element equations such as diagonal, and higher-order mass approximations, see Goudreau and Taylor[1973] and Fried [1979], but now tailored over a specified range of frequencies. A difficulty of such methods, is that they do not possess a firm mathematical basis for proving stability and convergence. In particular, they do not inherit the consistency inherent in the Galerkin method, an important ingredient for obtaining improved convergence rates with higher-order interpolation functions.

Over the last view years, a new class of residual based finite element formulations has emerged to counteract the stability problems and other numerical pathologies exhibited by the classical Galerkin method. These methods are developed by appending residuals of the Euler-Lagrange equations to the standard Galerkin variational equation. The added residual terms preserve the consistency inherent in the parent Galerkin method. Methods of this type were originally developed by Hughes and Brooks [1979], to improve the stability of numerical solutions for the advection-diffusion equation, and are referred to as 'streamline-upwind/Petrov-Galerkin' (SUPG) methods. For a review of SUPG type methods applied to advective-diffusive systems and fluid flow equations, see Hughes [1987] and Johnson [1986].

These ideas have since been extended by Hughes, Franca and Hulbert [1989], to the concept of Galerkin/Least-Squares (GLS) by appending residuals of the Euler-Lagrange equations in least-squares form to the standard Galerkin formulation. GLS finite element methods have been successfully employed in a wide variety of applications where enhanced stability and accuracy properties are needed, including problems governed by Navier-Stokes and the compressible Euler equations of fluid mechanics, Shakib and Hughes [1991] and the transient structural acoustics problem using the space-time formulation developed in this thesis.

Recently, Harari and Hughes [1991b] have applied GLS technology to the Helmholtz equation for one-dimensional model problems. An important feature of GLS methods is the introduction of a local mesh parameter into the variational equation that may be designed to provide accurate solutions with relatively coarse meshes. Harari and Hughes accomplished this for one-dimensional problems using dispersion analysis. In Harari and Hughes [1992c], the GLS mesh parameter derived in one-dimension is used in the DtN finite element method proposed by Keller and Givoli [1989] for solving the exterior Helmholtz problem. Although it was found that the one-dimensional parameter improved the accuracy of the Galerkin solution in some two-dimensional example problems, a comprehensive analysis of GLS dispersion characteristics in two-dimensions was unavailable.

In this work the selection of the optimal GLS mesh parameter for the multi-dimensional Helmholtz equation is considered, and leads to elements that exhibit improved accuracy. Optimal GLS methods for time-harmonic wave propagation in multi-dimensions were first introduced in Thompson and Pinsky [1993c], with extensions to exterior problems in THOMPSON AND PINSKY [1993d]. Although for any given direction of wave propagation, it is shown in this work that an optimal GLS mesh parameter can be obtained, in general, the direction of wave propagation will not be known *a priori*. To remedy this difficulty, a GLS parameter is found which reduces phase error for all possible wave vector directions over an element. By performing a multi-dimensional Fourier analysis we have been able to characterize the phase accuracy and directional properties of the Galerkin/Least-Squares solution over all wave vector magnitudes and directions. A number of alternative GLS parameters are derived for general numerical integration rules such as Gaussian and Lobatto quadrature and their dispersion characteristics analyzed over the full range of wave vector orientations. Results from this analysis quantify the reduction in phase error achieved using alternative GLS mesh parameters. A number of example problems are numerically solved to verify the accuracy of the GLS method and assess the performance of competing GLS design parameters. Extensions to three-dimensional trilinear elements are discussed as well as alternative methods such as the Generalized Galerkin/Least-Squares (GGLS) method. Extensions to higher-order finite element interpolations is also considered. In particular, an optimal GLS parameter is designed that reduces dispersion for elements with quadratic interpolation functions, together with some approximate GLS mesh parameters useful for efficient computation.

8.2 Overview

In Section 8.3 the Helmholtz equation and its characteristic equation relating frequency and wave vector components in two-dimensions is reviewed. In Section 8.4 the Galerkin/Least-Squares variational equation is given. Difference equations arising from the assembly of a uniform discretization of bilinear elements are derived in Section 8.5. In Section 8.6 a discrete Fourier analysis is performed. Optimal GLS parameters are derived and dispersion curves compared to the standard Galerkin method in Section 8.7. In Section 8.8, numerical examples of both interior and exterior problems are solved. Extensions of the new multi-dimensional GLS mesh parameters to three-dimensions and to Generalized Galerkin/Least-Squares (GGLS) methods are give in Sections 8.9.1 and 8.9.2 respectively. Finally in Section 8.9.3 the application of GLS methods to high-order finite element interpolations is considered.

8.3 The Helmholtz Equation

To illustrate the ideas involved for the selection of optimal Galerkin/Least-Squares mesh parameters in multi-dimensional wave propagation problems, we start with the two-dimensional Helmholtz equation; extensions to three-dimensions is straightforward.

Consider a two-dimensional homogeneous isotropic acoustic medium whose wave speed is c. The wave solution $u(\boldsymbol{x}, t)$ corresponding to a harmonic source vibrating at a given fixed frequency $\omega > 0$ satisfies the scalar wave equation:

$$\nabla^2\phi(\boldsymbol{x}, t) - \phi_{,tt}(\boldsymbol{x}, t)/c^2 = -f(\boldsymbol{x})e^{-i\omega t}, \qquad (\boldsymbol{x}, t) \in \Omega \times]0\,, T[\tag{8.24}$$

Looking for a solution to (8.24) such that $u(\boldsymbol{x}, t) = \phi(\boldsymbol{x})e^{-i\omega t}$ we find that ϕ must satisfy the scalar Helmholtz (reduced wave) equation:

$$\mathcal{L}\phi \equiv \nabla^2\phi + k^2\phi = -f \qquad \text{in} \;\; \Omega \tag{8.25}$$

where $k = \omega/c > 0$ is the wavenumber with wavelength $2\pi/k$, ∇^2 is the Laplacian differential operator and Ω is the spatial domain of interest.

The Helmholtz equation in $\mathbb{R}^2$ admits the plane-wave propagating solution,

$$\phi(x, y) = e^{i(k_x x + k_y y)} \tag{8.26}$$

where the frequency ω and the wave vector components k_x and k_y are linked by the characteristic equation,

$$\boxed{\left(\frac{\omega h}{c}\right)^2 = (k_x h)^2 + (k_y h)^2} \tag{8.27}$$

and h is a problem dependent characteristic length. This nondispersive relation is satisfied by the directional wave vector components $k_x = k\cos\theta$ and $k_y = k\sin\theta$, where the normal to the plane wave is oriented at angle θ relative to the x-axis.

Alternatively, the characteristic equation (8.27) can be obtained by a two-dimensional

Fourier transform from physical space to wave space through the transform operation,

$$\tilde{F}(k_x, k_y) := \frac{1}{\sqrt{2\pi}} \int_{-\infty}^{\infty} \int_{-\infty}^{\infty} F(x, y) \mathrm{e}^{-i(k_x x + k_y y)} dx dy \tag{8.28}$$

The discrete counterpart to this continuous transform will be used as a tool for the design of improved finite element methods for the solution of the two-dimensional Helmholtz equation.

8.4 Finite Element Formulations

Consider a partition of Ω into finite elements. Let Ω_e be the interior of the eth element, and $\tilde{\Omega} = \bigcup_e \Omega_e$. Let $\mathcal{S}^h \subset H^1(\Omega)$ and $\mathcal{V}^h \subset H^1(\Omega)$ be finite element spaces consisting of continuous piecewise polynomials of order p.

8.4.1 Galerkin

As a point of departure, consider the classical Galerkin method.
Given $k = \omega / c > 0$, *find* $\phi^h \in \mathcal{S}^h$, such that

$$A(w^h, \phi^h) = L(w^h) \qquad \forall w^h \in \mathcal{V}^h \tag{8.29}$$

where

$$A(w^h, \phi^h) \equiv (\nabla w^h, \nabla \phi^h)_\Omega - k^2 (w^h, \phi^h)_\Omega \tag{8.30}$$

$$L(w^h) \equiv (w^h, f)_\Omega \tag{8.31}$$

and $(\cdot, \cdot)_\Omega$ denotes the $L_2(\Omega)$ inner product. The Galerkin formulation is consistent in the sense that ϕ, the exact solution to the Helmholtz equation, satisfies (8.29). For $k^2 > 0$ the operator,

$$A(w^h, w^h) = ||\nabla w^h||^2 - k^2 ||w^h||^2 \qquad \forall w^h \in \mathcal{V}^h \tag{8.32}$$

loses positive-definiteness as the wavenumber increases, resulting in a loss of ellipticity (stability) with increasing wavenumber. This difficulty is especially important when solving large-scale problems with iterative solvers where the condition number of the matrix equations, and hence the convergence rate, depends on the wavenumber, see for example, Bayliss, Goldstein, and Turkel [1983].

8.4.2 Galerkin/Least-Squares

It is well known that the phase accuracy associated with the Galerkin finite element solution degrades as the wavenumber k is increased relative to the mesh parameter h. In order to improve the accuracy characteristics of the standard Galerkin method, a least-squares operator is added to (8.29). This additional operator is constructed from a residual of the governing Helmholtz differential equation evaluated within element interiors.

$$\boxed{A(w^h, \phi^h) + (\tau \mathcal{L} w^h, r^h)_{\tilde{\Omega}} = L(w^h)} \tag{8.33}$$

In this expression, $r^h = \mathcal{L}\phi^h + f$ is the residual, and τ is a local mesh parameter with units of inverse length-squared to be determined from dispersion analysis. If $\tau = 0$, the method reverts to Galerkin. Formally, GLS can be stated as follows:
Find $\phi^h \in \mathcal{S}^h$, *such that*

$$A_{GLS}(w^h, \phi^h) = L_{GLS}(w^h) \qquad \forall w^h \in \mathcal{V}^h \tag{8.34}$$

where

$$A_{GLS}(w^h, \phi^h) \equiv A(w^h, \phi^h) + \sum_{e=1}^{n_{el}} \int_{\Omega_e} \tau \mathcal{L} w^h \, \mathcal{L}\phi^h \, d\Omega \tag{8.35}$$

$$L_{GLS}(w^h) \equiv L(w^h) - \sum_{e=1}^{n_{el}} \int_{\Omega_e} \tau \mathcal{L} w^h \, f \, d\Omega \tag{8.36}$$

As a result of being a weighted residual method, the error $e = \phi^h - \phi$ is orthogonal $\forall w^h \in \mathcal{V}^h$ with respect to A_{GLS}.

$$A_{GLS}(w^h, e) = 0 \tag{8.37}$$

This consistency condition is an important ingredient in obtaining improved convergence rates with higher-order interpolation. A Fourier synthesis of A_{GLS} from physical space to wavenumber space is used as a tool to determine the optimal τ for two-dimensional applications.

8.4.3 Illustration of fundamental difficulty

The following calculations demonstrates the difficulty Galerkin methods have in resolving time-harmonic waves as the wavenumber is increased relative to the mesh size. Consider the problem of finding the solution $\phi : \bar{\Omega} = \{(x,y) : 0 \leq x \leq L_x, 0 \leq y \leq L_y\} \rightarrow \mathbb{R}$ with an inhomogeneous Dirichlet boundary condition within a waveguide.

$$(\nabla^2 + k^2)\phi(x,y) = 0 \qquad \text{in } \Omega \tag{8.38}$$

$$\phi(0,y) = g_0, \qquad \phi(L_x,y) = 0 \tag{8.39}$$

$$\phi_{,y}(x,0) = \phi_{,y}(x,L_y) = 0 \tag{8.40}$$

The analytical solution to this problem is characterized by the standing plane-wave representation,

$$\phi(x|k) = g_0 \frac{\sin(k(L_x - x))}{\sin(kL_x)} \tag{8.41}$$

Let $L_x = L_y = L$, and discretize the computational domain with a uniform mesh of $n_{el} = 10 \times 10$ equally spaced bilinear finite elements. It can be verified that the GLS nodal solution to this problem has the same form as the analytical solution but with the physical wavenumber k replaced with a numerical wavenumber k^h. Since this problem is an example of a plane-wave solution directed along x-direction mesh lines, the problem essentially is one-dimensional. In this case the GLS method can be designed to achieve nodal exactness (superconvergence) by choosing an optimal GLS parameter τ such that exact phase is obtained, that is $k^h = k$, Harari and Hughes [1991b].

Figure 8.1 illustrates the elevated contours of the nodally exact GLS solution interpolated with the underlying mesh, for a nondimensional wavenumber $kh = \pi/6$, corresponding to a relatively refined mesh of twelve elements per wavelength. The profile of this solution plotted along the x-axis is shown in Figure 8.2(top). The Galerkin ($\tau = 0$) solution with either consistent ($\epsilon = 1$) or lumped mass ($\epsilon = 0$) approximation is well-resolved as predicted from the finite element dispersion analysis

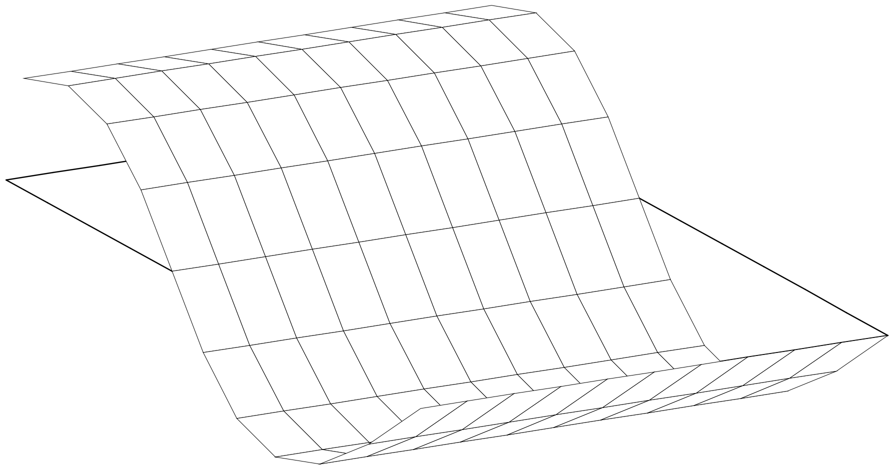

Figure 8.1: Elevated contours of plane-wave solution directed along x-direction mesh lines with $kh = \pi/6$, twelve elements per wavelength.

in the following Sections. Figure 8.2(bottom) illustrates that as the wavenumber is increased to $kh = \pi/3$, corresponding to a coarse mesh of six elements per wavelength, the accuracy of the Galerkin solution deteriorates significantly, while GLS remains nodally exact as designed.

For a uniform mesh of piecewise linear finite elements, then $\nabla^2\phi^h$ is identically zero on element interiors, and with no sources $f = 0$, the method reverts to a modified wavenumber method, i.e.

$$A_{GLS}(w^h, \phi^h) = (\nabla w^h, \nabla \phi^h)_\Omega - \tilde{k}^2(w^h, \phi^h)_\Omega \tag{8.42}$$

where $\tilde{k}^2 \equiv (1-\tau k^2)k^2$. If $f \neq 0$, the GLS method differs from a modified wavenumber approach in that the consistent loading operator for GLS takes the form,

$$L_{GLS}(w^h) = (1 - \tau k^2)L(w^h) \tag{8.43}$$

This distinction is crucial in order to maintain the consistency and accuracy of the GLS formulation. As an illustration of this issue, consider the same problem as above

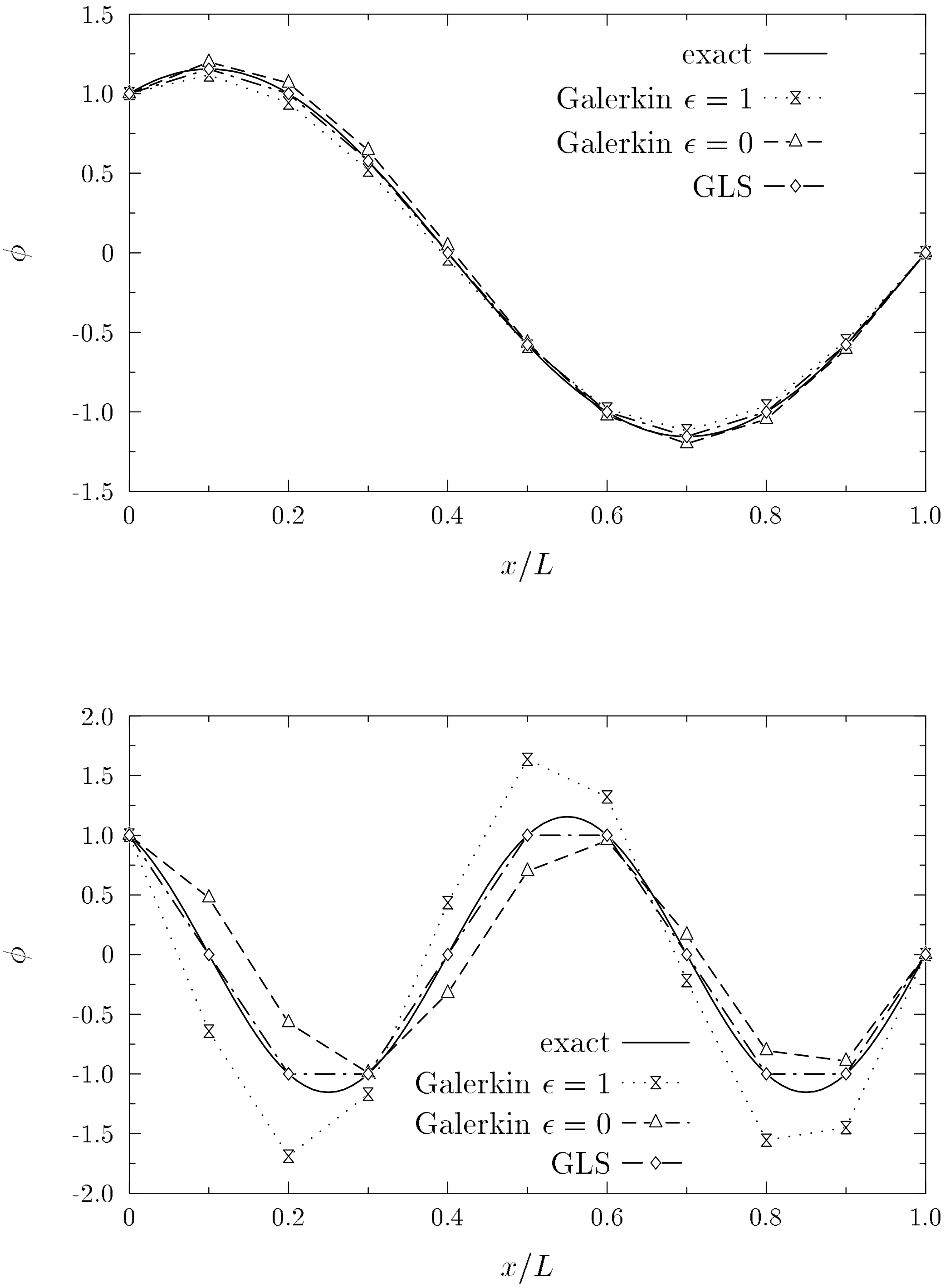

Figure 8.2: Waveguide problem with plane-wave solution directed along x-direction mesh lines with (top) $kh = \pi/6$, twelve elements per wavelength. (bottom) $kh = \pi/3$, six elements per wavelength.

but now with a source loading given by $f = -10\sin(2\pi x/L)$, and a nondimensional wavenumber $kh = \pi/3$ corresponding to six elements per wavelength. Figure 8.3 shows that when source terms are present, i.e. $f \neq 0$, then a modified wavenumber approach becomes inconsistent and as a result loses accuracy. In contrast, the GLS method, with consistent modification of the loading operator maintains nodal exactness by design. To this authors knowledge, this is the first demonstration of this fact for the Helmholtz equation. While for plane-waves traveling along mesh lines it is possible to obtain nodally exact solutions, in multi-dimensional wave propagation problems, this is not generally possible. The goal of this work then is to design an optimal GLS mesh parameter for multi-dimensional waves that minimizes dispersion errors over all possible wave vector orientations.

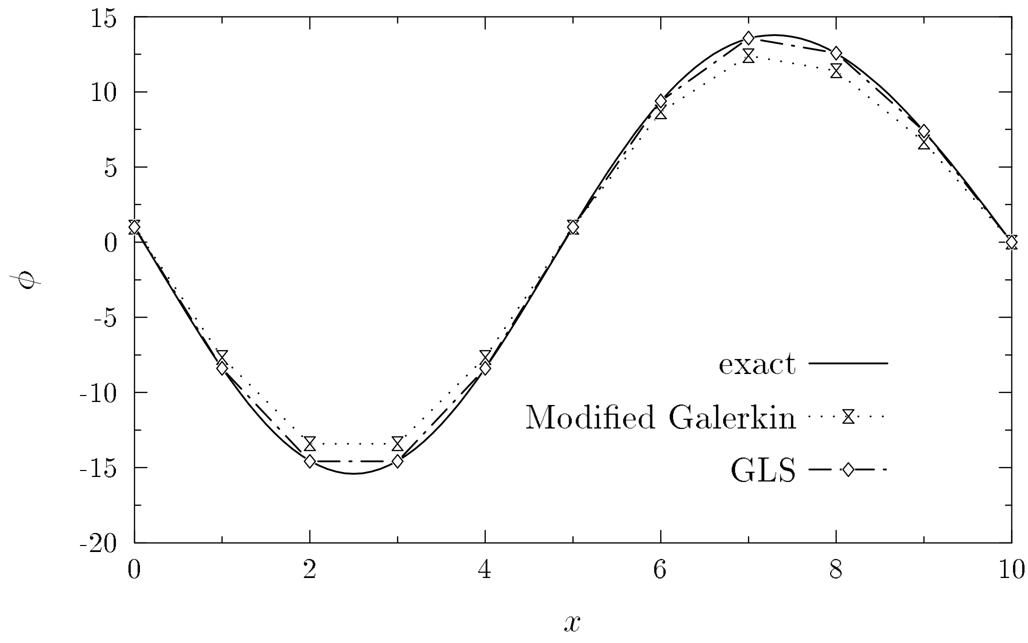

Figure 8.3: Waveguide problem with source term $f = -10\sin(2\pi x/L)$, and $kh = \pi/3$, six elements per wavelength.

8.5 Finite Element Discretization

Consider a uniform mesh of bilinear elements,

$$\mathbb{R}_h^2 = \{(x, y) \in \mathbb{R}^2 = (mh_x, nh_y), (m, n) \in \mathbb{Z}\} \tag{8.44}$$

with element sides h_x in the x-direction and h_y in the y-direction. In order to expose the directional behavior of the finite element discretization, the approximation of ϕ^h and w^h within each element is defined as the tensor product $\mathcal{P}^1 \times \mathcal{P}^1$ of one-dimensional linear interpolants over the biunit square $(\xi, \eta) \in (-1, 1)^2$:

$$\phi^h(\xi, \eta) = \sum_{k=1}^{2} \sum_{l=1}^{2} L_k(\xi) L_l(\eta) \phi_{kl}^e \tag{8.45}$$

$$w^h(\xi, \eta) = \sum_{i=1}^{2} \sum_{j=1}^{2} L_i(\xi) L_j(\eta) w_{ij}^e \tag{8.46}$$

where $L_i(\xi) = (1 + \xi_i \xi)/2$, $\xi_i = \pm 1$ and $\phi_{kl}^e = \phi^h(\xi_k, \eta_l)$ are the element nodal variables. For a uniform mesh of bilinear elements, all derivatives of order higher that one vanish within element interiors Ω^e, i.e. $\mathcal{L}\phi^h = k^2 \phi^h$. When $f = 0$, the GLS local element equations defined in tensor product form are,

$$\sum_k \sum_l \left(S_{ijkl}^e - \gamma k^2 M_{ijkl}^e \right) \phi_{kl}^e = 0 \tag{8.47}$$

The quantity

$$\boxed{\gamma := (1 - \tau k^2)} \tag{8.48}$$

embodies the GLS mesh parameter τ, and the local element stiffness and mass tensors integrated with a (2×2) quadrature rule are defined as,

$$\boldsymbol{S}^e = [S_{ijkl}^e], \qquad S_{ijkl}^e := \frac{1}{h_x^2} A_{ik} B_{jl} + \frac{1}{h_y^2} B_{ik} A_{jl} \tag{8.49}$$

$$\boldsymbol{M}^e = [M_{ijkl}^e], \qquad M_{ijkl}^e := B_{ik} B_{jl}/4 \tag{8.50}$$

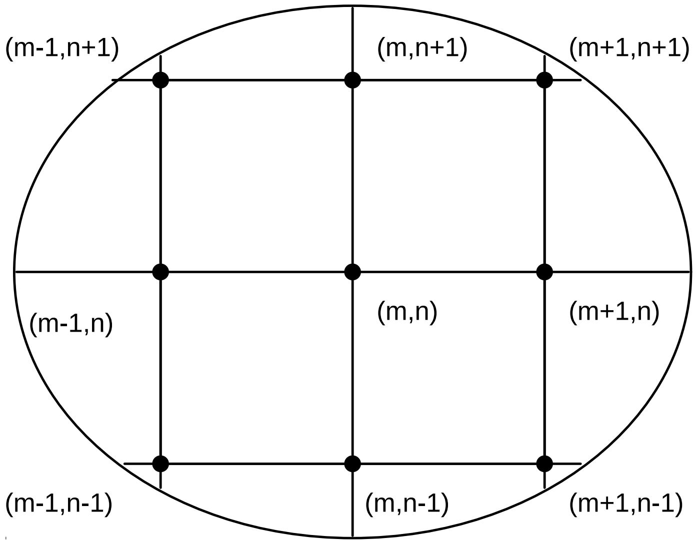

Figure 8.4: Two-dimensional bilinear finite element mesh with spacing $\Delta x = h_x$ and $\Delta y = h_y$.

where the discrete L_2 inner products are given by,

$$A^e_{ij} = \sum_{q=1}^{2} L'_i(\xi_q) L'_j(\xi_q) W_q, \qquad B^e_{ij} = \sum_{q=1}^{2} L_i(\xi_q) L_j(\xi_q) W_q \tag{8.51}$$

and ξ_q is the quadrature point and W_q the quadrature weight. In these expressions the prime on the shape functions denotes differentiation. For (2×2) Gaussian quadrature, the inner products are exactly integrated. For Lobatto quadrature, B^e_{ij} is underintegrated and diagonal, i.e. $B^e_{ij} = \delta_{ij}\, W_j$.

Finite element difference relations are obtained by assembling a patch of four bilinear elements as illustrated in Figure 8.4. The result is the difference stencil associated with the interior node $\phi_{m,n} = \phi^h(mh_x, nh_y)|\mathbb{R}^2_h \mapsto \mathbb{C}$.

$$\boxed{F(k) = S\phi_{m,n} - \gamma k^2 M \phi_{m,n} = 0} \tag{8.52}$$

where S and M are the two-dimensional linear difference operators emanating from the assembled stiffness (discrete Laplacian) and mass tensors respectively.

$$S = \sum_{p,q=-1}^{1} s_{pq} E_x^p E_y^q = S_x + S_y \tag{8.53}$$

$$S_x = -\frac{1}{h_x^2}(1 + \frac{\epsilon}{6}\delta_y^2)\delta_x^2 \tag{8.54}$$

$$S_y = -\frac{1}{h_y^2}(1 + \frac{\epsilon}{6}\delta_x^2)\delta_y^2 \tag{8.55}$$

$$M = \sum_{p,q=-1}^{1} m_{pq} E_x^p E_y^q = M_x \times M_y \tag{8.56}$$

$$M_x = (1 + \frac{\epsilon}{6}\delta_x^2) \tag{8.57}$$

$$M_y = (1 + \frac{\epsilon}{6}\delta_y^2) \tag{8.58}$$

The directional shift operators are defined by,

$$E_x^p \phi_{m,n} = \phi_{m+p,n} \qquad \text{and} \qquad E_y^q \phi_{m,n} = \phi_{m,n+q} \tag{8.59}$$

and the central difference operators are defined by,

$$\delta_x^2 \phi_{m,n} = \phi_{m-1,n} - 2\phi_{m,n} + \phi_{m+1,n} \tag{8.60}$$

$$\delta_y^2 \phi_{m,n} = \phi_{m,n-1} - 2\phi_{m,n} + \phi_{m,n+1} \tag{8.61}$$

The ϵ is a general quadrature parameter equal to 1 for exact Gaussian quadrature and 0 for Lobatto quadrature. The mass operator M is referred to as consistent when $\epsilon = 1$ and lumped when $\epsilon = 0$. Expressions for the bilinear stiffness and mass stencils $[s_{pq}]$ and $[m_{pq}]$ defined for the interior node (m,n) using consistent mass are given by,

$$[s_{pq}] = -\frac{1}{6h_x^2}\begin{bmatrix} 1 & -2 & 1 \\ 4 & -8 & 4 \\ 1 & -2 & 1 \end{bmatrix} - \frac{1}{6h_y^2}\begin{bmatrix} 1 & 4 & 1 \\ -2 & -8 & -2 \\ 1 & 4 & 1 \end{bmatrix}$$

$$[m_{pq}] = \frac{1}{36}\begin{bmatrix} 1 & 4 & 1 \\ 4 & 16 & 4 \\ 1 & 4 & 1 \end{bmatrix}$$

8.6 GLS Dispersion Relations

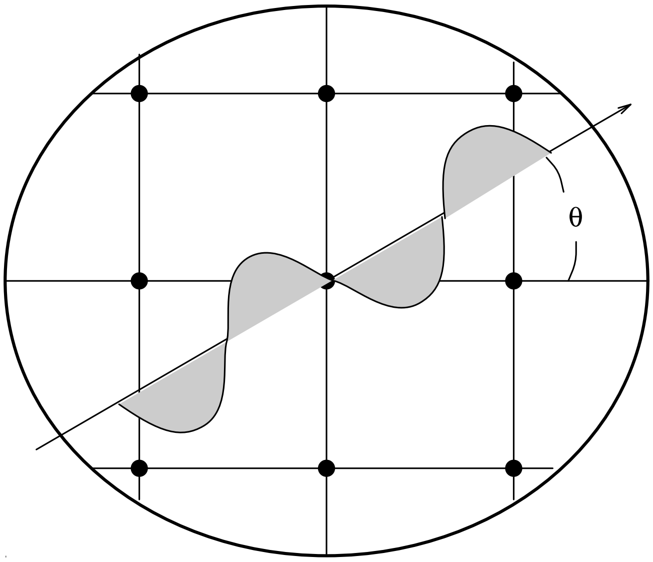

Figure 8.5: Direction of plane-wave with angle θ measured relative to mesh lines

The GLS finite element dispersion relations are obtained by assuming a plane-wave solution propagating at an arbitrary angle relative to the mesh lines,

$$\phi_{m,n} = \mathrm{e}^{i(k_x^h h_x m + k_y^h h_y n)} \tag{8.62}$$

with $i = \sqrt{-1}$. In the above, the directional wave vector components are denoted $k_x^h = k^h \cos\theta$ and $k_y^h = k^h \sin\theta$ with numerical wavenumber k^h. The normal is oriented at angle θ relative to mesh lines, see Figure 8.5. Substituting (8.62) into (8.52) results in the following GLS dispersion relation,

$$\boxed{\tilde{F}(k, k_x^h, k_y^h) = \tilde{S} - \gamma k^2 \tilde{M} = 0} \tag{8.63}$$

This equation describes the relationship between the continuous wavenumber $k = \omega/c$ and the finite element discrete wave vector components k_x^h and k_y^h. In this relation, $\tilde{S}$ and $\tilde{M}$ represent the discrete Fourier transforms of the linear difference operators S and M respectively. Expressions for these transformed stiffness and mass operators are given by,

$$\tilde{S}(k_x^h h_x, k_y^h h_y) = \sum_{p,q=-1}^{1} s_{pq} \mathrm{e}^{i(k_x^h h_x p + k_y^h h_y q)} = \mathbf{1}_y \bar{k}_x^2 + \mathbf{1}_x \bar{k}_y^2 \tag{8.64}$$

$$\tilde{M}(k_x^h h_x, k_y^h h_y) = \sum_{p,q=-1}^{1} m_{pq} \mathrm{e}^{i(k_x^h h_x p + k_y^h h_y q)} = \mathbf{1}_x \mathbf{1}_y \tag{8.65}$$

with notation,

$$\bar{k}_x^2 = 2(1 - f_x)/h_x^2 \qquad \text{and} \qquad \bar{k}_y^2 = 2(1 - f_y)/h_y^2 \tag{8.66}$$

$$\begin{aligned} f_x &= \cos(k_x^h h_x) = \cos(k^h h_x \cos\theta) \\ f_y &= \cos(k_y^h h_y) = \cos(k^h h_y \sin\theta) \end{aligned}$$

$$\mathbf{1}_x = 1 - \frac{\epsilon}{6}(\bar{k}_x h_x)^2 \qquad \text{and} \qquad \mathbf{1}_y = 1 - \frac{\epsilon}{6}(\bar{k}_y h_y)^2 \tag{8.67}$$

For a detailed description of the discrete Fourier transform applied to linear difference equations, see Vichnevetsky and Bowles [1982]. The characteristic equation (8.63) describes the nonlinear relationship between the continuous wavenumber $k = \omega/c$ and the finite element discrete wave vector components k_x^h and k_y^h. Written in the alternate form,

$$\gamma k^2 = D^h(k^h, \theta), \qquad D^h = \tilde{S}/\tilde{M} \tag{8.68}$$

it is clear that the dispersion relation depends on both the magnitude of the discrete wavenumber $k^h := |k^h|$ and the orientation of the wavevector θ.

$$|k^h| = \sqrt{(k_x^h)^2 + (k_y^h)^2} \tag{8.69}$$

$$\theta = \tan^{-1}(k_y^h / k_x^h) \tag{8.70}$$

8.7 Selection of an optimal GLS mesh parameter

The optimal least-squares mesh parameter τ is obtained by requiring the phase to be exact, i.e. $k = k^h$ for any choice of wave vector angle $\theta = \theta_o$. This requirement is met by replacing k^h with the exact wavenumber, $k = \omega/c$, in the GLS finite element dispersion relation (8.68), restricting $h_x = h_y = h$, and solving for γ. With this design criteria, the optimal τ is defined as,

$$\boxed{\tau k^2 := 1 - \frac{\tilde{S}(kh, \theta_o)}{k^2 \tilde{M}(kh, \theta_o)}} \tag{8.71}$$

where $\tilde{S}$ and $\tilde{M}$ are defined in (8.64) through (8.67) with k^h replaced with $k = \omega/c$. In particular, for exact 2×2 Gaussian integration, the expression for the optimal GLS mesh parameter is,

$$\boxed{\tau k^2 = 1 - \frac{6(4 - f_x - f_y - 2f_x f_y)}{(kh)^2(2 + f_x)(2 + f_y)}} \tag{8.72}$$

Selecting $\theta_0 = 0$, (8.71) specializes to,

$$\tau k^2 := 1 - \frac{6(1 - \cos kh)}{(kh)^2(3 - \epsilon(1 - \cos kh))} \tag{8.73}$$

which yields exact phase for plane-waves directed along uniform mesh lines. When $\epsilon = 1$ this definition specializes to the GLS parameter derived by Harari and Hughes [1991b] in one-dimension. For comparison the GLS mesh parameter τ defined in (8.72), with $\epsilon = 1$, designed to give exact phase for plane-waves oriented along $\theta = 0$ (denoted τ_0) and $\theta = 22.5$ (denoted $\tau_{22.5}$) are plotted in Figure 8.6. For reference, $kh/\pi = 0.2$ represents a mesh with ten elements per wavelength. In this range, the two τ parameters compared are nearly identical and close to zero. Thus, when there are more than ten elements per wavelength, the least-squares contribution has only a small effect on the Galerkin solution. At $kh/\pi = 0.4$, corresponding to only five elements per wavelength, the two GLS parameters compared show a significant difference.

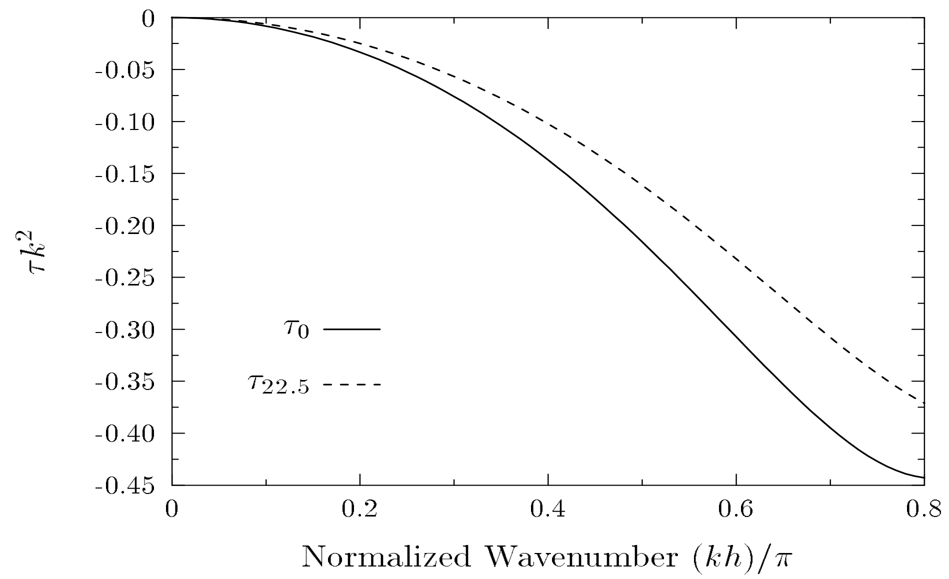

Figure 8.6: Optimal GLS parameters designed to give exact phase for plane waves directed along $\theta = 0$ (denoted τ_0), and $\theta = 22.5$ (denoted $\tau_{22.5}$).

8.7.1 GLS dispersion analysis

In this section, the performance of alternate GLS mesh parameters, based on definition (8.71), with different choices of θ_o and ϵ are examined. The accuracy of the numerical solution is assessed in terms of the phase error defined by,

$$\mathrm{e}_p(k^h, \theta) := \frac{k}{k^h} \tag{8.74}$$

with $\omega = kc = k^h c^h$, we can write the phase error in the alternative form $\mathrm{e}_p = c^h/c$. Exact phase corresponds to $\mathrm{e}_p = 1$. Results are plotted for plane wave solutions directed along mesh lines $\theta = 0$, and for plane wave solutions directed along mesh diagonals $\theta = 45$. Results for orientations $\theta \in]0, 45[$ are bounded by these angles.

8.7.2 Consistent mass

Dispersion curves for Galerkin $\tau = 0$ and GLS with τ_0, designed to give exact phase for plane-waves directed along $\theta = 0$ are given in Figure 8.7. Results are given for plane-waves propagating at angles $\theta = 0$, 22.5 and 45. Near the origin, the relative phase speed converges to unity $\mathrm{e}_p = 1$, but as the wavenumber increases, the phase error also increases. The Galerkin solution exhibits a phase lead $c^h/c > 1$ and the

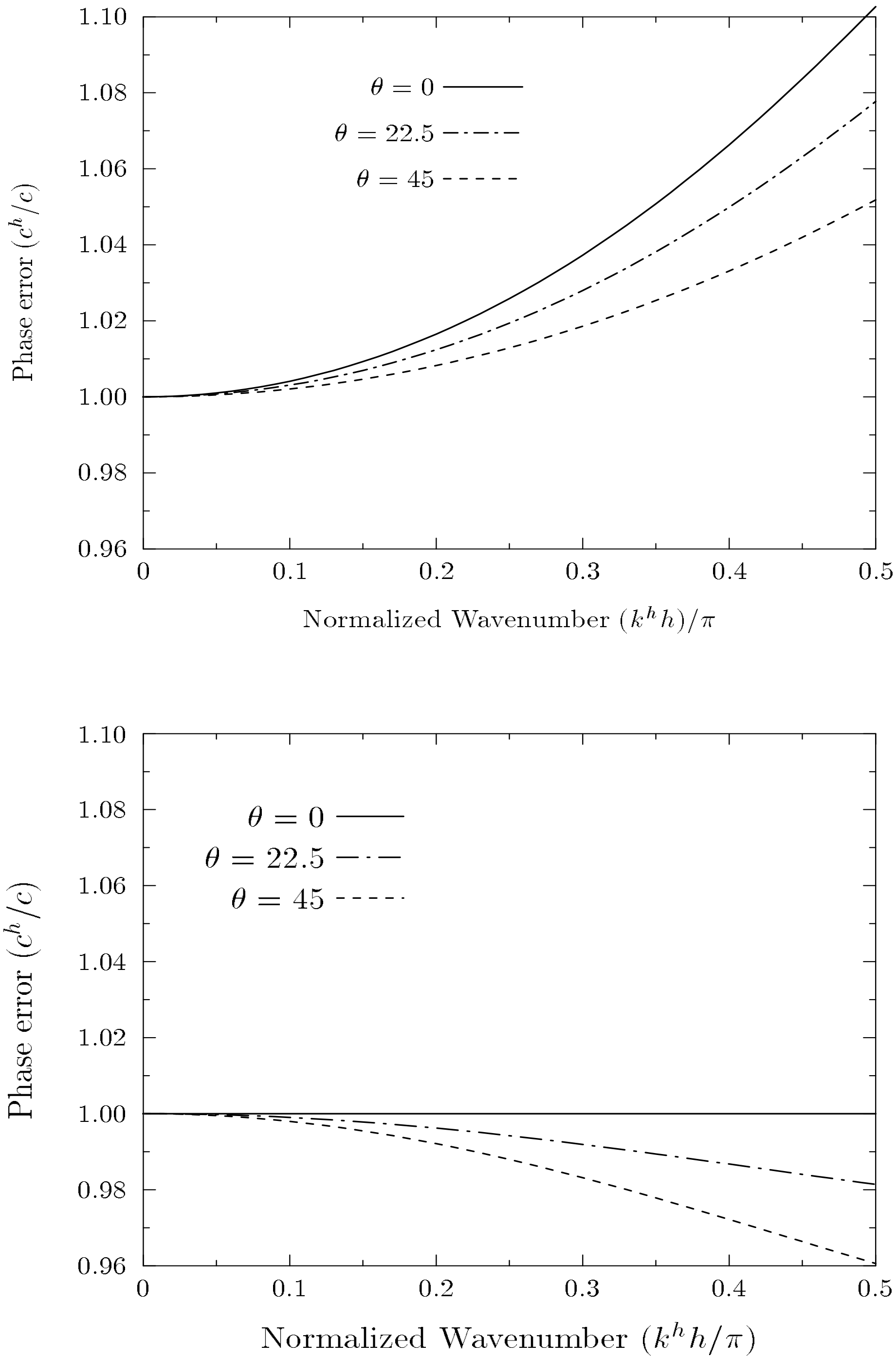

Figure 8.7: Phase error at three different angles $\theta = 0$, 22.5 and 45 using exact integration for (top) Galerkin $\tau = 0$, (bottom) GLS $\tau = \tau_0$, designed to give exact phase for $\theta = 0$.

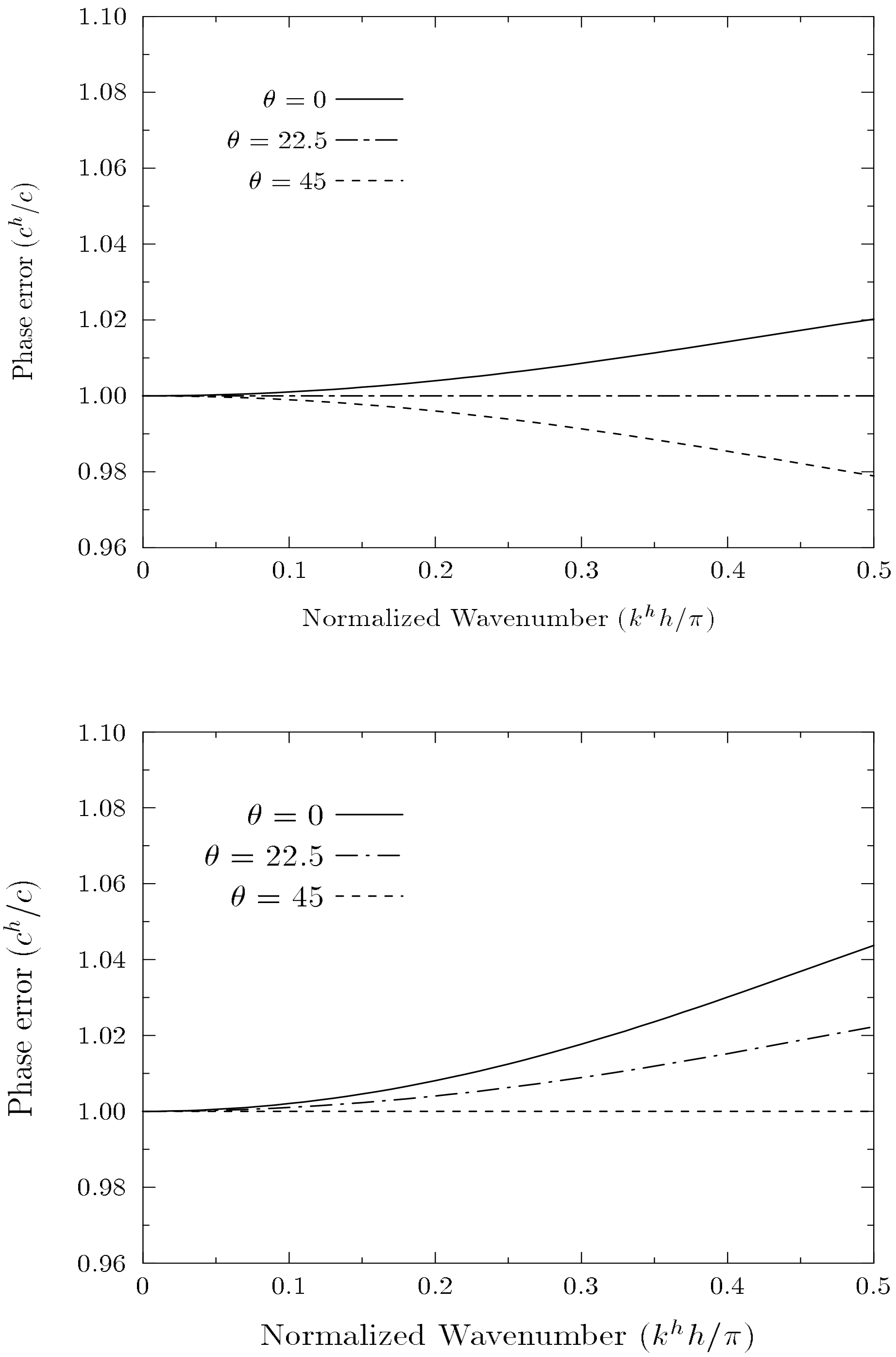

Figure 8.8: Phase error using exact integration for (top) GLS $\tau = \tau_{22.5}$, (bottom) GLS $\tau = \tau_{45}$

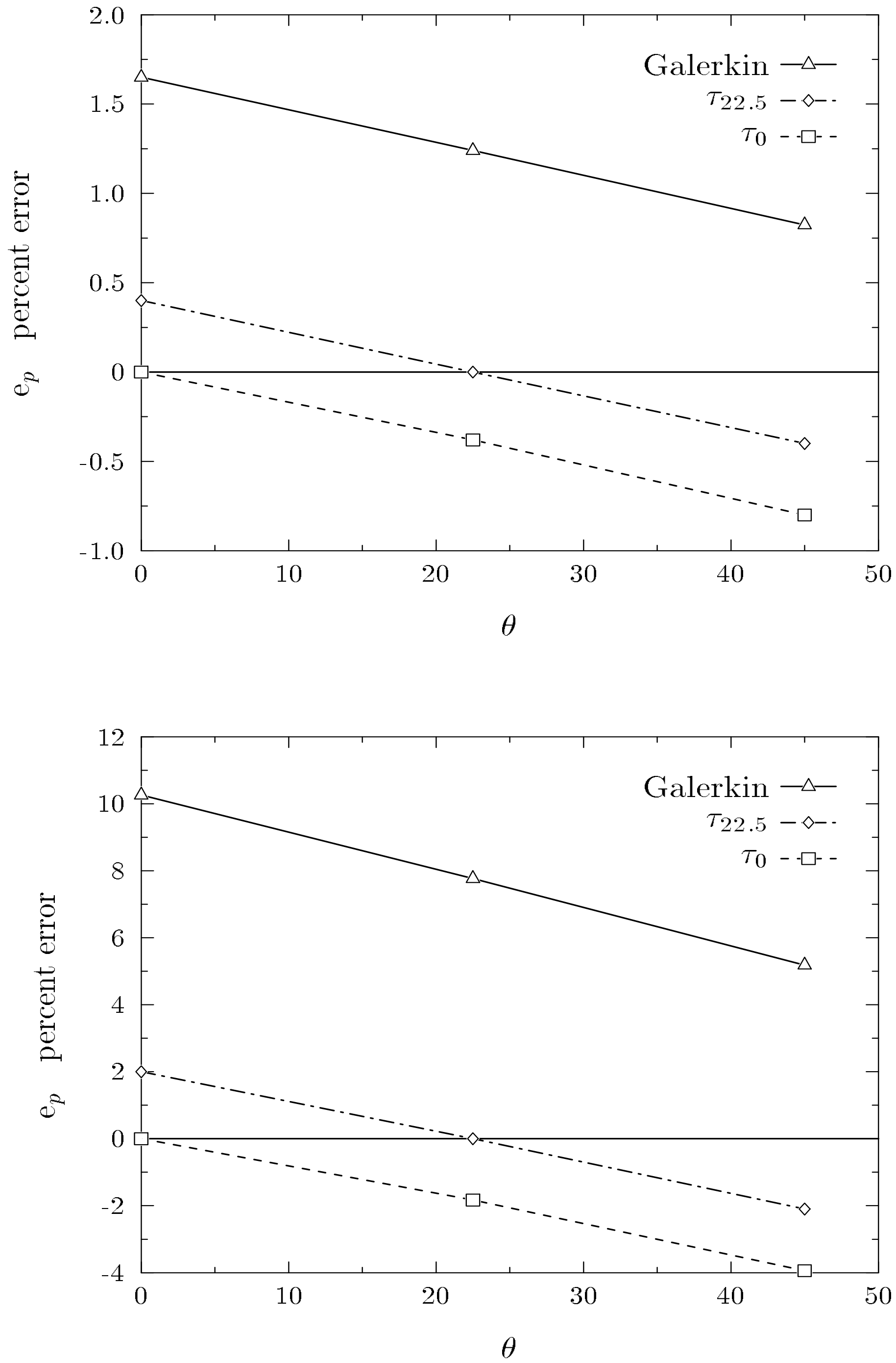

Figure 8.9: Phase error using exact integration at (top) 10 elements per wavelength, (bottom) 4 elements per wavelength.

phase error is a minimum for plane-waves directed along mesh diagonals $\theta = 45$. For a mesh refinement of ten elements per wavelength ($k^h h = .2\pi$), the maximum phase error max$|\mathrm{e}_p|$ evaluated over all angles θ is less than 2 percent. As the wavenumber is increased relative to the mesh parameter h, the phase accuracy degrades severely to max$|\mathrm{e}_p| = 10$ percent. For GLS with τ_0 and exact integration, the two-dimensional GLS dispersion relation relating the exact wavenumber $k = \omega/c$, to the discrete wavenumber k^h and angle θ is given by,

$$kh = \cos^{-1}\left\{\frac{4(f_x + f_y) + 5f_x f_y - 4}{f_x + f_y - f_x f_y + 8}\right\} \tag{8.75}$$

By design, for propagation along mesh lines $\theta = 0$ (mod 90), this relation reduces to the exact phase relationship $\mathrm{e}_p = 1$ for $kh \in (0, \pi)$. Referring to Figure 8.7, the dispersion curves for $\theta \neq 0$ exhibit a phase lag $c^h/c < 1$ with max$|\mathrm{e}_p|$ reduced to approximately 4 percent at four elements per wavelength. These two-dimensional dispersion results show how the addition of the least-squares operator, with the GLS mesh parameter τ_0 defined in (8.73), reduces the phase error over all wave vector orientations θ.

In Figure 8.8, the dispersion curves for the alternative GLS parameters, $\tau_{22.5}$ designed for exact phase at $\theta = 22.5$, and τ_{45} designed for exact phase at $\theta = 45$ are compared. For τ_{45}, the maximum phase error is still approximately 4 percent but is now reflected about the exact solution $c^h/c = 1$ such that there is a phase lead $c^h/c > 1$. By choosing the GLS parameter $\tau_{22.5}$, corresponding to exact phase for $\theta = 22.5$, the envelope of the dispersion curves is centered around the exact result $c^h/c = 1$. As a result, the GLS solution exhibits a maximum possible error $|\mathrm{e}_p|$ of only 2 percent at four elements per wavelength as compared to 10 percent for Galerkin. At ten elements per wavelength, GLS with $\tau_{22.5}$ has a maximum possible error of 0.5 percent, compared to 1.6 percent for Galerkin. Figure 8.9 illustrates these conclusions from an alternative viewpoint. In this Figure, the phase error is plotted versus the angle of wave propagation; comparisons are made with Galerkin ($\tau = 0$) and GLS with ($\tau_{22.5}$) and (τ_0) at ten elements per wavelength (top), and four elements per wavelength (bottom). These results clearly show that the solution with $\tau_{22.5}$ gives exact phase for propagation angles $\theta = 22.5$, while the solution with τ_0 gives exact phase for propagation angles $\theta = 0$. The phase error for GLS with τ_0 is a minimum (exact) at $\theta = 0$, and then increases to a maximum of 4 percent at $\theta = 45$. Phase accuracy is increased for $\tau_{22.5}$, where the maximum error is only 2 percent at $\theta = 0$ and $\theta = 45$.

In conclusion, firstly, it is clear that the least-squares addition with τ defined by (8.71) substantially improves the phase accuracy of the finite element solution for any choice of wave vector orientation θ. Secondly, we find that when the direction of wave-propagation is not known *a priori*, or when it is varying over the mesh, as will generally be the case, then $\tau_{22.5}$ is optimal.

8.7.3 Diagonal mass

The effectiveness of the Galerkin/Least-Squares method when using a lumped mass approximation (Lobotto quadrature) is examined by setting $\epsilon = 0$ in (8.73), with the result

$$\tau k^2 = 1 - \frac{2(1 - \cos kh)}{(kh)^2} \tag{8.76}$$

The two-dimensional GLS dispersion relation in this case is,

$$kh = \cos^{-1}\left\{(f_x + f_y + 2f_x f_y - 1)/3\right\} \tag{8.77}$$

Figure 8.10 plots dispersion curves using a lumped mass approximation for Galerkin and GLS with the τ defined in (8.76). These results confirm that the least-squares addition is effective for improving the phase accuracy of Galerkin solutions even when approximate quadrature rules are used to integrate the mass operator.

8.8 Numerical Studies

A number of numerical studies are conducted to verify the improved accuracy of the GLS method and assess the performance of alternate GLS mesh parameters.

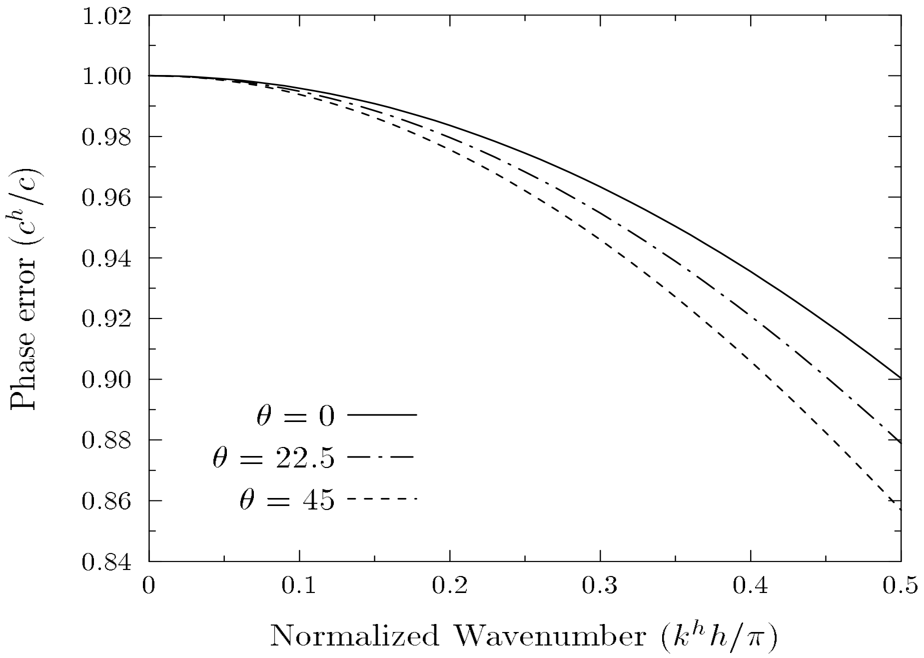

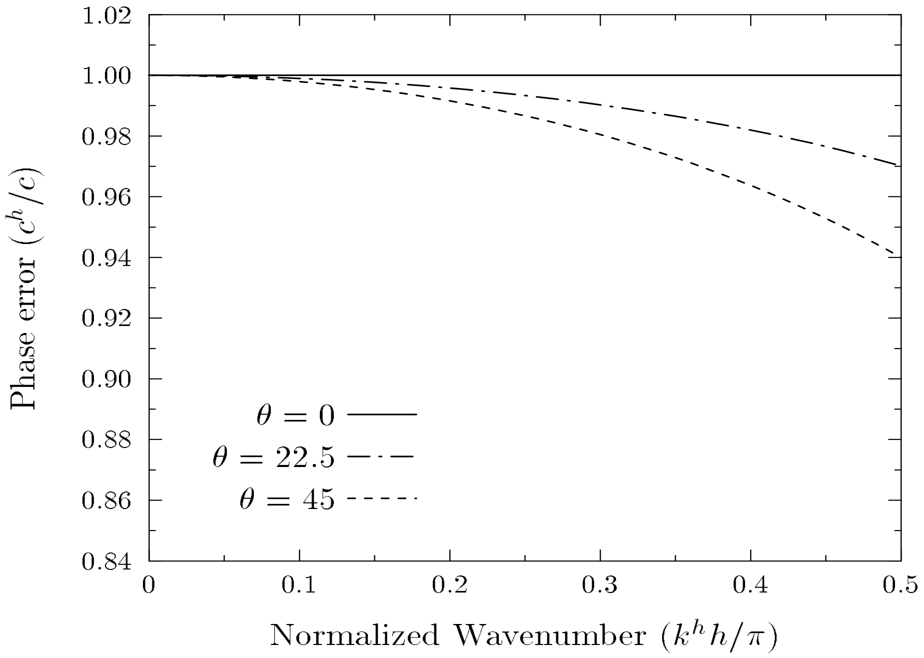

Figure 8.10: Phase error using diagonal mass approximation, $\epsilon = 0$, (top) Galerkin ($\tau = 0$) (bottom) GLS ($\tau = \tau_0$), designed for exact phase for $\theta = 0$.

8.8.1 Green's function for a rectangular domain

In this first example, consider the problem of finding the Green's function $\phi : \bar{\Omega} \to \mathbb{R}$ with homogeneous Dirichlet boundary conditions within a square domain.

$$(\nabla^2 + k^2)\phi(x,y) = -\delta(x - x_0, y - y_0) \qquad \text{in } \Omega \tag{8.78}$$

$$\phi(0,y) = \phi(L,y) = \phi(x,0) = \phi(x,L) = 0 \tag{8.79}$$

where L is the side length. The solution to this problem is composed of a series of reflected waves which give rise to complicated standing wave patterns, see THOMPSON AND PINSKY [1993d].

This problem is numerically solved by the Galerkin/Least-Squares method using a uniform mesh of 20×20 bilinear quadrilateral elements. All calculations are performed with 2×2 Gauss integration with $kL = 5\pi/3$. The source is located in the upper right quadrant $(x_0, y_0) = (0.8L, 0.8L)$. In the upper left corner of Figure 8.11 the elevated contours of the exact series solution interpolated with the mesh employed is illustrated. In the figures that accompany this result, the contours of the exact, Galerkin and GLS ($\tau_{22.5}$) solutions are shown respectively. The solution profile for a cut located at $y = 0.2L$ is given in Figure 8.12. The L_2 norm of the error evaluated over all nodal points excluding the source node is computed as,

$$||e||^2 = \sum_m \sum_n (\phi^h_{mn} - \phi(x_m, y_n))^2 \tag{8.80}$$

The computed values of $||e||$ for Galerkin and GLS using the mesh parameters τ_0 and $\tau_{22.5}$ are:

$$\begin{aligned} \text{Galerkin} &= 0.691 \\ \text{GLS}(\tau_0) &= 0.240 \\ \text{GLS}(\tau_{22.5}) &= 0.148 \end{aligned}$$

Results of this numerical example indicate that the additional least-squares operator with the family of mesh parameters τ defined in (8.71) improves the accuracy of the Galerkin solution. However, for problems where waves are directed in arbitrary directions in $\mathbb{R}^2$, use of the GLS parameter $\tau_{22.5}$ is more accurate than the use of τ_0. These results substantiate the conclusions drawn from the multi-dimensional dispersion analysis of the previous section: If the predominant direction θ, is known *a priori*, then the optimal mesh parameter can be calculated from (8.71). However, for general problems where waves are directed in arbitrary directions in $\mathbb{R}^2$, use of the GLS parameter $\tau_{22.5}$ is more accurate than the use of τ_0.

8.8.2 Plane-wave propagation in a waveguide

Next, consider the problem of plane-wave propagation along a waveguide. The set-up for this problem is the same as given in (8.38) through (8.40), but now with the finite element mesh rotated at 45 degrees relative to the rectangular boundaries, see Figure 8.13. This example illustrates that for problems where the direction of wave propagation is known *a priori*, in this case along the x-axis, the optimum GLS parameter τ can be calculated from (8.71). For this mesh and loading, the greatest accuracy is obtained by choosing τ such that $\theta_o = 45$ since the mesh lines are rotated by 45 degrees to the direction of propagation. The GLS solution to this problem is illustrated in Figure 8.14. For comparison, the Galerkin and GLS solutions using τ_{45}; exact for waves directed along $\theta = 45$ relative to mesh lines and $\tau_{22.5}$; exact for waves directed along $\theta = 22.5$ are also shown in this Figure. From this result we observe that the GLS solution with τ_{45} is very close to the nodal interpolate of the exact solution. The solution is not perfectly nodally exact for this mesh due to the presence of linear triangular elements used near the boundaries. Results for the alternative GLS parameter $\tau_{22.5}$ also exhibit significantly improved phase accuracy when compared to Galerkin.

8.8.3 Effects of mesh distortion

In studies by Bazant and Celep [1978,1982], finite element solutions over non-uniform meshes exhibit reflections at mesh discontinuities that can cause increased amplitude and phase errors. Although undistorted (uniform) meshes tend to minimize errors due to reflection at mesh discontinuities, it is often desirable to employ unstructured meshes in an adaptive scheme to capture gradients in the solution amplitude near for example irregular surfaces or source drivers. To investigate the effects

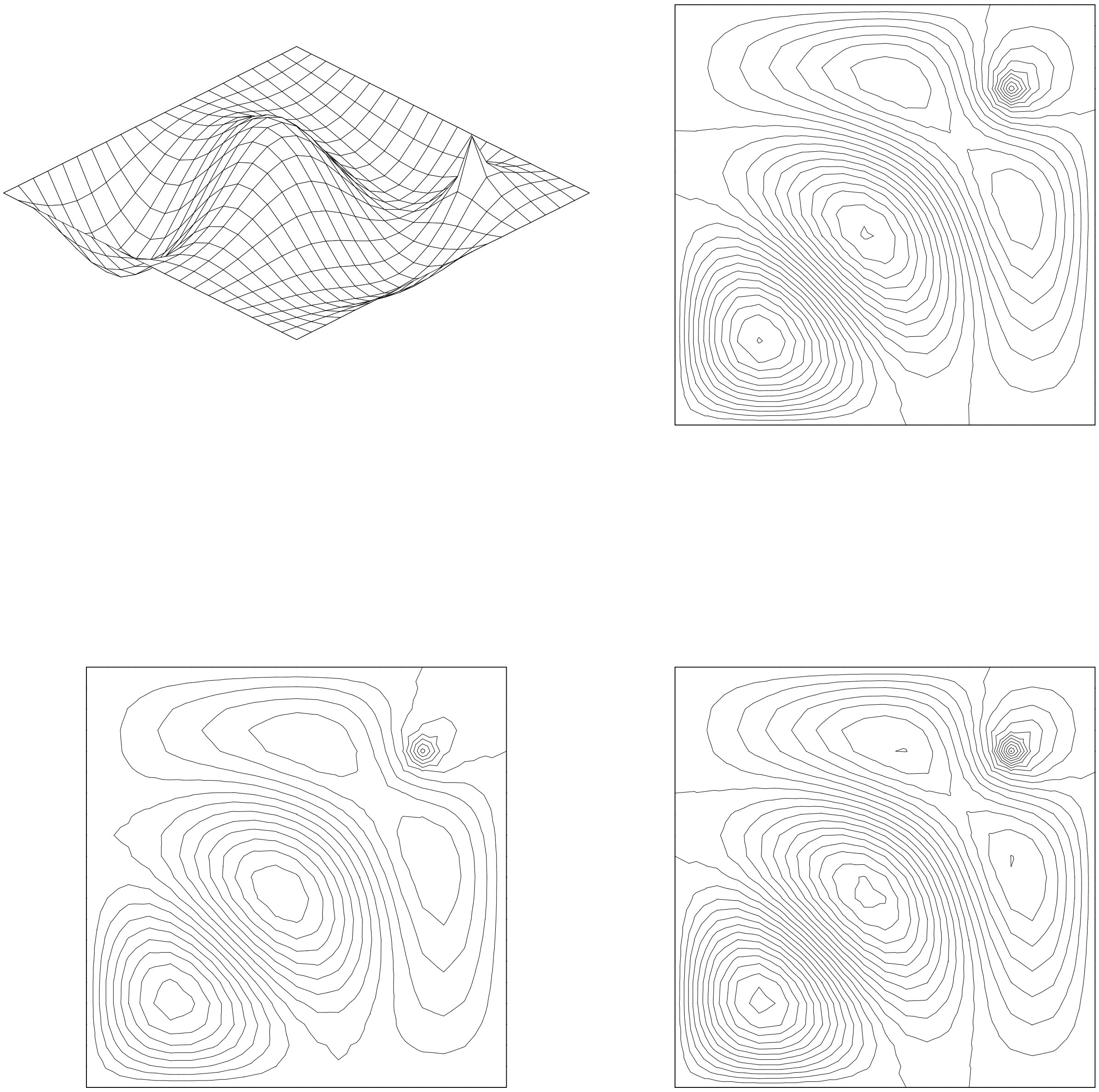

Figure 8.11: Contours for point source located in upper right quadrant of a uniform mesh of (20×20) bilinear elements, at $kL = 5\pi/3$. (Upper left) Elevated contours for exact series solution. (Upper right) Contours of exact solution, (Bottom left) Galerkin, (Bottom right) Galerkin/Least-Squares

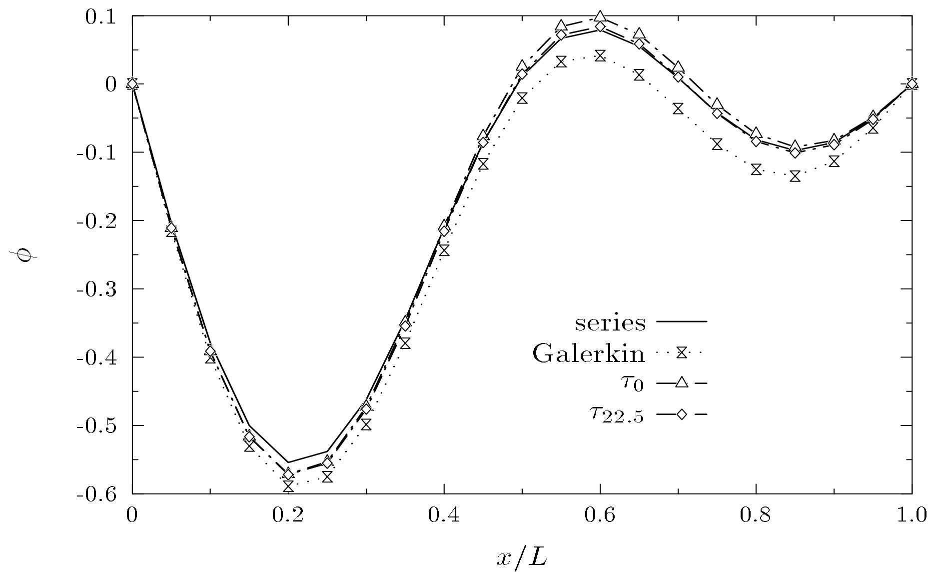

Figure 8.12: Point source located in upper right quadrant: Solution profile along x–axis for fixed $y/L = 0.2$

of mesh distortion on the Galerkin/Least-Squares solution, the uniform mesh used in the previous example is distorted such that the element area remains fixed, see Figure 8.15. For this problem, the element length h is chosen to be the square-root of the element area. In order to compare results with the nodes spaced at uniform points, the projection algorithm described in JANSEN [1992] is used to linearly interpolate the unstructured nodes to the structured nodes. Figure 8.16 shows that while the GLS numerical solution with the distorted mesh is no longer nodally exact, it it remarkably accurate. This example illustrates that at least for a quisi-uniform discretization of distorted elements, the GLS method performs optimally. However, further studies need to be performed in order to assess the accuracy and stability of the GLS technology to truly unstructured meshes with no uniformity in the mesh.

8.8.4 Radiation from an infinite cylinder

Currently there is intense interest in the application of analytical and numerical techniques to model exterior wave propagation problems such as the radiation and scattering of acoustic waves from geometrically complex structures. In this example, consider

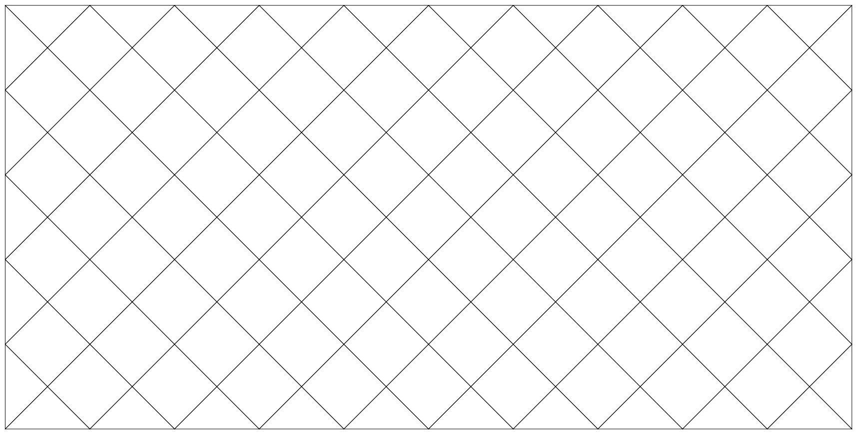

Figure 8.13: Rotated finite element mesh of linear quadrilateral elements and linear triangular elements for waveguide problem.

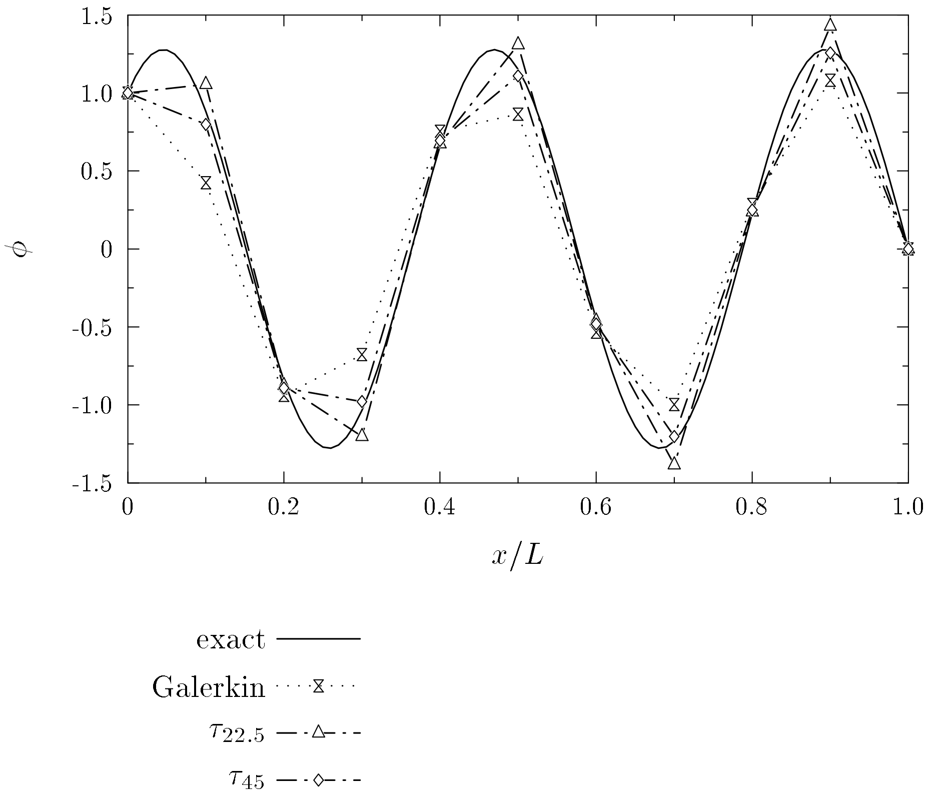

Figure 8.14: Waveguide problem with rotated mesh and plane-wave solution directed along x-axis; $kh = \pi/3$, six elements per wavelength.

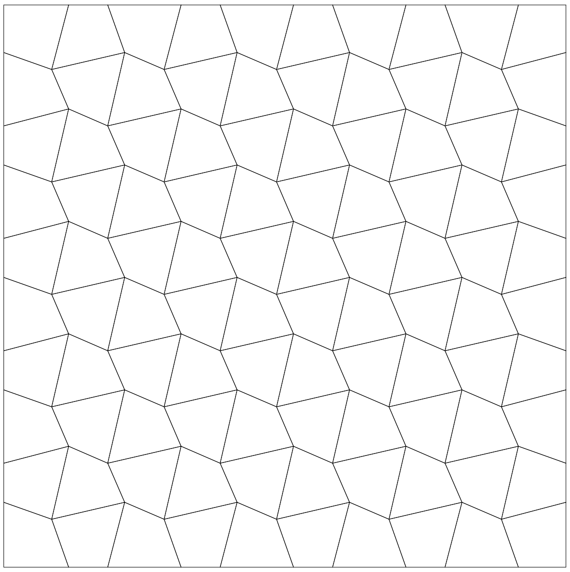

Figure 8.15: The computational domain for a square waveguide with length L, discretized by a distorted mesh of 10×10 bilinear quadrilateral elements.

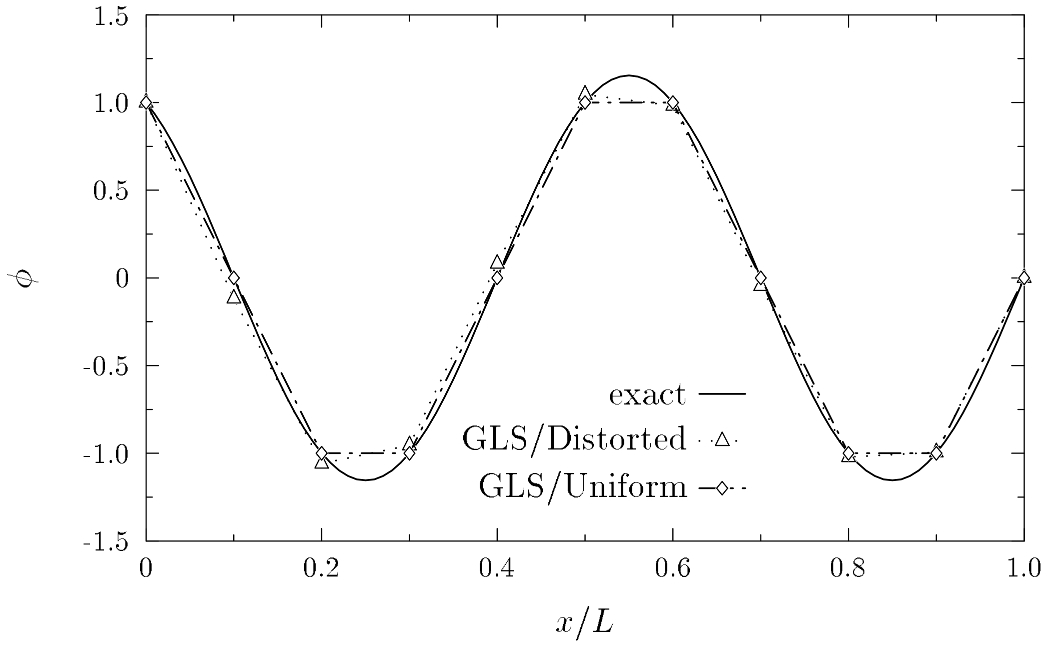

Figure 8.16: Waveguide problem with plane-wave solution directed along x-direction; comparing uniform and distorted meshes, for $kh = \pi/3$, six elements per wavelength:

the problem of non-uniform radiation from a rigid infinite cylinder of radius a. By increasing the circumferential harmonic loading on the surface of the cylinder, the response of individual modes on the performance of the numerical solution is examined. For this exterior problem, the solution $\phi : \mathcal{R} = \{a \leq r < \infty, 0 \leq \theta < 2\pi\} \rightarrow \mathbb{C}$, is sought such that,

$$(\nabla^2 + k^2)\phi(r,\theta) = 0 \qquad \text{in } \mathcal{R} \tag{8.81}$$

$$\phi(a,\theta) = \cos n\theta \tag{8.82}$$

$$\lim_{r\rightarrow\infty} \sqrt{r}(\phi,_r - ik\phi) = 0 \tag{8.83}$$

The exact solution to this problem is $H_n(kr)\cos n\theta/H_n(ka)$ where H_n are Hankel functions of the first kind of order n.

This problem is solved by the GLS finite element method by truncating the infinite domain at a finite distance from the cylinder with an artificial boundary. A non-reflecting boundary condition representing the impedance of the exterior domain is then prescribed at this artificial boundary. Let the artificial boundary to be a circle of radius R. The problem defined over the bounded domain Ω is then:
Find $\phi : \Omega = \{a \leq r \leq R, 0 \leq \theta < 2\pi\} \rightarrow \mathbb{C}$, such that

$$(\nabla^2 + k^2)\phi(r,\theta) = 0 \qquad \text{in } \Omega \tag{8.84}$$

$$\phi(a,\theta) = \cos n\theta \tag{8.85}$$

$$\phi,_r(R,\theta) = \mathbb{S}\phi(R,\theta) \tag{8.86}$$

where the last equation is the non-reflecting boundary condition expressed through the Dirichlet-to-Neumann (DtN) mapping $\mathbb{S}$. The exact DtN map $\mathbb{S}$, is expressed as the infinite series,

$$\mathbb{S}\phi = \sum_{n=0}^{\infty} \alpha_n \int_0^{2\pi} \cos n(\theta - \theta')\phi(R,\phi')d\phi' \tag{8.87}$$

where the impedance coefficients are defined as,

$$\alpha_n(kR) := \frac{\varepsilon_n k}{\pi}\frac{H_n'(kR)}{H_n(kR)} \tag{8.88}$$

and ε_n is equal to 1/2 for $n = 0$ and 1 otherwise. This non-local non-reflecting boundary condition in the frequency domain was used earlier in Chap. 5, as a starting point for the derivation of local boundary conditions in the time domain. Here we implement this nonlocal DtN condition directly as a natural boundary condition in the GLS variational formulation for the Helmholtz equation. Further details pertaining to implementation of the DtN boundary condition in a finite element formulation are given in KELLER AND GIVOLI [1989] and GIVOLI AND KELLER [1989].

For this example the positioning of the truncation boundary is set at $R = 2a$ with the resulting computational domain discretized by 3×32 bilinear quadrilateral elements as shown in the upper left had corner of Figure 8.17. In the following calculations the geometrically non-dimensionalized wavenumber is set at $ka = \pi$ (the wavelength is equal to the diameter of the cylinder). With the finite element mesh employed, this value corresponds to a resolution of six elements per wavelength in the radial direction. All calculations employ 2×2 Gaussian integration and 8 terms in the DtN series.

For the first harmonic (breathing mode $n = 0$), the exact solution is a simple cylindrical wave which has the character of a radially decaying plane-wave. For the radially uniform mesh employed, this problem reduces to a one dimensional problem with radial coordinate r. Taking h to be the element length in the r-direction, HARARI AND HUGHES [1992c] have shown that the GLS parameter τ_0 is optimal in this case.

In this work, the higher-order circumferential harmonics $n = 1$ through $n = 4$ are investigated in order to further validate the accuracy of the GLS method for more complex non-uniform radiation patterns. In the upper left corner of Figure 8.17 the contours of the imaginary part of the exact solution for the loading $\cos\theta$, nodally interpolated by the mesh employed is shown. The contours of the imaginary parts of the Galerkin and GLS solutions are shown in the accompaning figures, where comparisons are made to the exact solution which is denoted by the overlay of dotted contours. Figure 8.18 shows the profile of the solution evaluated on the DtN boundary $r = R$ for modes $n = 1$ through $n = 3$. The GLS solution was calculated using both τ_0 and $\tau_{22.5}$ defined previously.

For mode $n = 1$, the improvement of the GLS solutions in comparison to the Galerkin solution is significant. We also observe that in this case, τ_0 is superior to $\tau_{22.5}$. As the circumferential mode is increased to $n = 2$, the improvement to the GLS

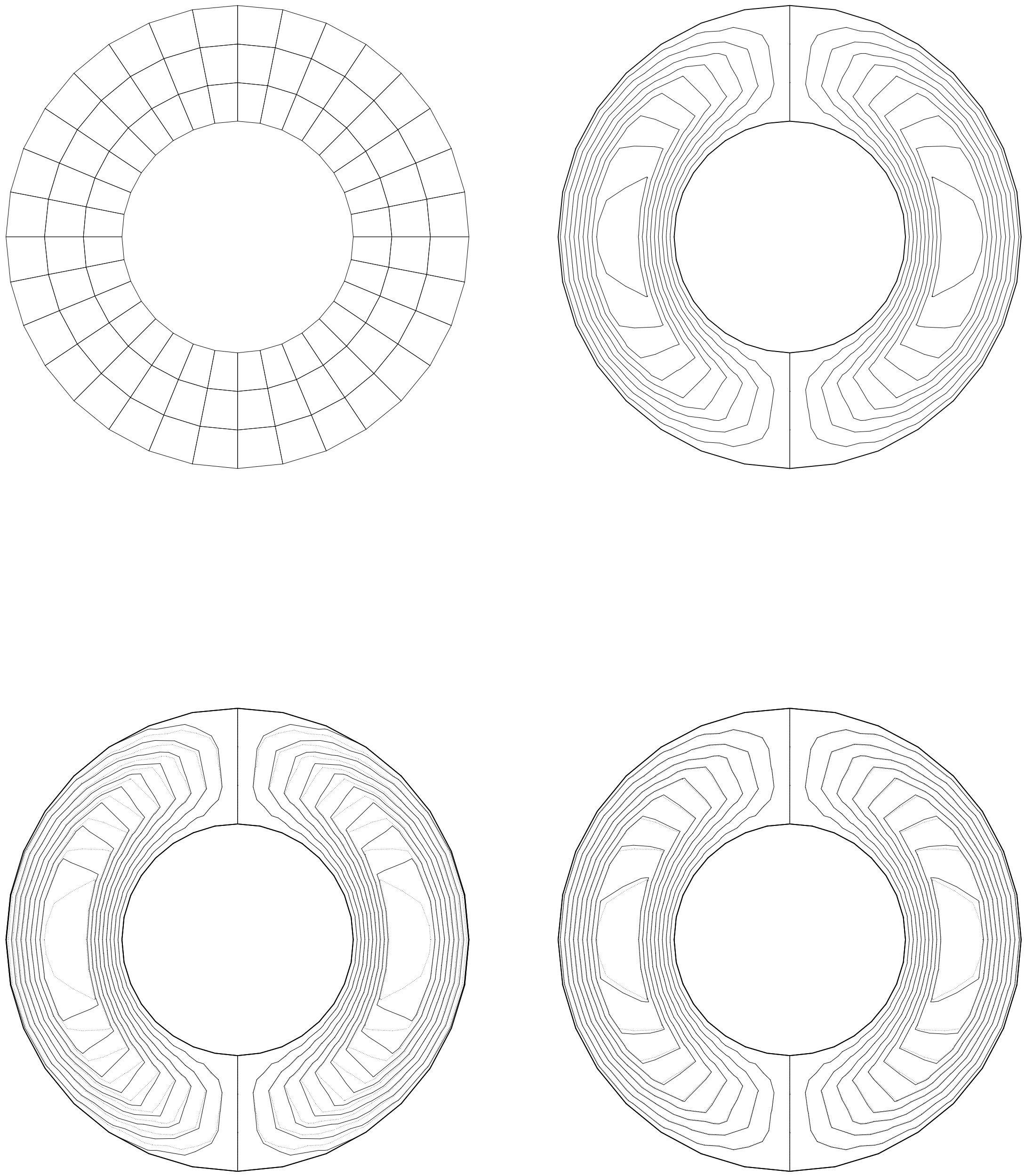

Figure 8.17: Harmonic radiation with mode ($n = 1$) and $ka = \pi$: (Upper left) Computational domain for a cylinder with radius a, and truncation boundary $R = 2a$. (top right) Exact solution (bottom left) Galerkin solution (bottom right) Galerkin/Least-Squares with $\tau_{22.5}$

solution is again significant, however in this case, the GLS solution using either τ_0 or $\tau_{22.5}$ are nearly identical. The use of τ_0 slightly under-estimates the exact solution while the use of $\tau_{22.5}$ slightly over-estimates the exact solution. For mode $n = 3$, the improvement of the GLS solutions in comparison to the Galerkin solution is again clearly shown. However, in this case the use of $\tau_{22.5}$ gives the most accurate solution and is barely distinguishable from the exact solution. Results for mode $n = 4$ are given in Thompson and Pinsky [1993d].

The results of this study indicate that for this particular problem, for low modes $n = 0, 1$, the radiated energy of the cylindrical waves are best resolved by the GLS parameter τ_0, designed to improve dispersion errors for plane-waves directed along radial rays, while for higher modes $n = 3, 4$, the alternative GLS parameter $\tau_{22.5}$ designed for arbitrary directional wave vectors performs better. In more general settings such as radiation from a source located on a geometrically complex structure, the radiation pattern may be complex and difficult to predict a-priori. For these more general problems, a radially uniform mesh may not be possible and unstructured meshes must be used. In the case of unstructured meshes, it is expected that $\tau_{22.5}$ would give the best results, at least in a global sense. Further numerical studies need to be performed in order to verify this hypothesis.

8.9 Extensions of GLS

8.9.1 Three-dimensional elements

The selection of an optimal GLS parameter in three-dimensions is a simple extension of the two dimensional case. Consider a uniform mesh of trilinear 8-node brick elements with element sides h. The optimal τ in this case is,

$$\boxed{\tau k^2 := 1 - \frac{\tilde{S}(kh, \theta, \varphi)}{(kh)^2 \tilde{M}(kh, \theta, \varphi)}} \tag{8.89}$$

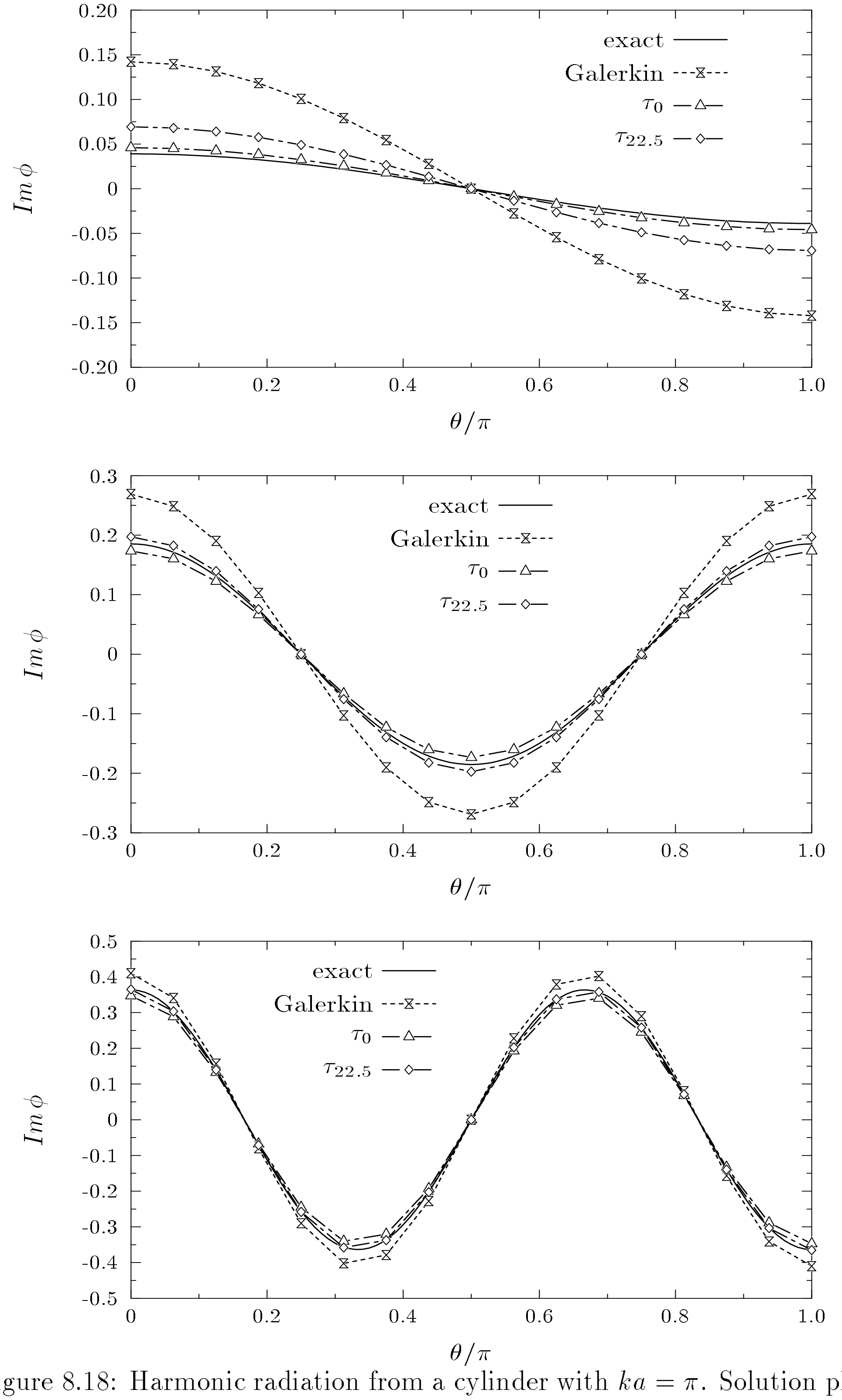

Figure 8.18: Harmonic radiation from a cylinder with $ka = \pi$. Solution plotted along the truncation boundary $R = 2a$. From top to bottom, mode $n = 1, 2, 3$

where $\tilde{S}$ and $\tilde{M}$ are the three-dimensional Fourier transforms of the stiffness and mass difference stencils respectively,

$$\tilde{S} = \mathbf{1}_y \mathbf{1}_z \bar{k}_x^2 + \mathbf{1}_x \mathbf{1}_z \bar{k}_y^2 + \mathbf{1}_x \mathbf{1}_y \bar{k}_z^2 \qquad \text{and} \qquad \tilde{M} = \mathbf{1}_x \mathbf{1}_y \mathbf{1}_z \tag{8.90}$$

$$\bar{k}_x^2 = 2(1 - f_x) \qquad \text{and} \qquad \bar{k}_y^2 = 2(1 - f_y) \qquad \text{and} \qquad \bar{k}_z^2 = 2(1 - f_z) \tag{8.91}$$

$$\begin{aligned} f_x &= \cos(k_x h) = \cos(kh \cos\theta \sin\varphi) \\ f_y &= \cos(k_y h) = \cos(kh \sin\theta \sin\varphi) \\ f_z &= \cos(k_z h) = \cos(kh \cos\varphi) \end{aligned}$$

with polar angles $\theta \in [0, 2\pi]$ and meridional angles $\varphi \in [0, \pi]$ measured relative to mesh axis. For $\varphi = 0$ mod 90, (8.89) specializes to the two-dimensional case (8.71). Further details for the three-dimensional case will be published in a follow-up paper to Thompson and Pinsky [1993d].

8.9.2 Generalized Galerkin Least Squares

Alterative variants on the theme of adding least squares terms to the usual Galerkin method are possible. Consider the following Generalized Galerkin/Least-Squares (GGLS) method in $\mathbb{R}^2$, where the added least-squares term is in the form of the gradient of the residual:

$$A_{GGLS}(w^h, \phi^h) \equiv A(w^h, \phi^h) + \sum_{e=1}^{n_{el}} \int_{\Omega^e} \boldsymbol{\tau} \nabla(\mathcal{L} w^h) \cdot \nabla(\mathcal{L} \phi^h) d\Omega \tag{8.92}$$

$$L_{GGLS}(w^h) \equiv L(w^h) - \sum_{e=1}^{n_{el}} \int_{\Omega^e} \boldsymbol{\tau} \nabla(\mathcal{L} w^h) \cdot \nabla f d\Omega \tag{8.93}$$

where $\mathcal{L}\phi^h = \phi^h_{,xx} + \phi^h_{,yy} + k^2 \phi^h$ and $\boldsymbol{\tau} = \mathrm{diag}(\tau_x, \tau_y)$ is a diagonal matrix of local parameters. Note that consistency is preserved since the exact solution satisfies the gradient of the Helmholtz equation. Setting $\tau_x = \tau_y = \tau$, the method reverts to the Galerkin Gradient Least Squares (G∇LS) method originally proposed by Franca and Dutra Do Carmo [1989], see also Harari [1991a] and Grosh and Pinsky

[1993b]. For bilinear elements and $f = 0$, the dispersion relations for this method are,

$$(kh)^2 \mathbf{1}_x \mathbf{1}_y = (1 + \tau_x k^4)\mathbf{1}_y \bar{k}_x^2 + (1 + \tau_y k^4)\mathbf{1}_x \bar{k}_y^2 \tag{8.94}$$

Restricting $\tau_x = \tau_y = \tau$, the GGLS dispersion relation reverts to,

$$(1 + \tau k^4)^{-1}(kh)^2 = \tilde{S}/\tilde{M} \tag{8.95}$$

which has the same form as equation (8.63) with $\gamma = (1 + \tau k^4)^{-1}$ and the optimal GGLS parameter is given by,

$$\boxed{\tau k^4 := \frac{(kh)^2 \tilde{M}(kh, \theta_0)}{\tilde{S}(kh, \theta_0)} - 1} \tag{8.96}$$

Examining (8.95) we conclude that for bilinear elements on a uniform grid with $f = 0$, the phase accuracy for GGLS with $\tau_x = \tau_y$ is identical to GLS over all wave vector orientations, and no advantage results. This observation was also made by Harari [1991a] for the one-dimensional case.

8.9.3 Biquadratic elements

While the 4-node bilinear discretizations represent popular element families due to their computational efficiency, higher-order elements such as biquadratic interpolations offer special advantages when solving the Helmholtz equation in two-dimensions. Higher-order elements better approximate the geometric curvature of a model description, and for time-harmonic wave solutions to the Helmholtz equation, increased phase accuracy will be realized for the same number of degrees of freedom as compared to low-order elements. In this section, the extension of the Galerkin/Least-Squares method for the Helmholtz equation to higher-order interpolations is presented.

As a point of departure we first consider the dispersive properties of high-order elements based on the Galerkin formulation for the Helmholtz equation.

Consider a uniform mesh of biquadratic ($\mathcal{P}^2 \times \mathcal{P}^2$) elements with length $h = 2\Delta x = 2\Delta y$. For simplicity, consider the Galerkin method where $\tau = 0$. By assembling a patch of four elements as shown in Figure 8.19, we identify four different difference

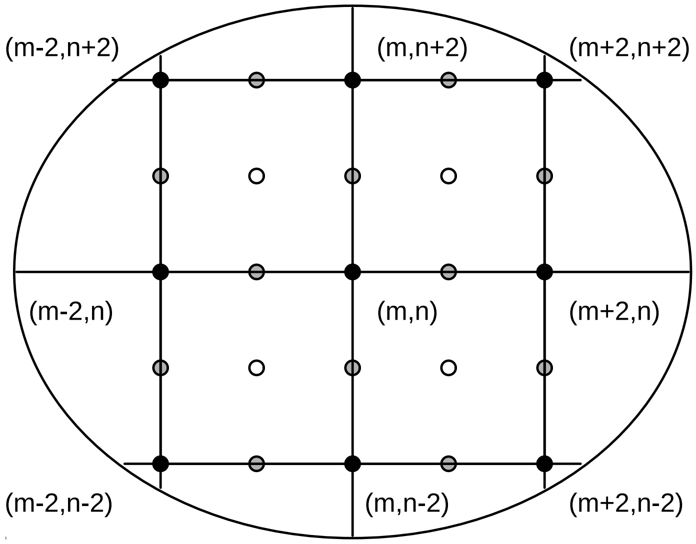

Figure 8.19: Two-dimensional biquadratic finite element mesh with corner, edge, and internal nodes.

stencils, each having the form,

$$\boxed{\sum_{p,q}(s_{pq} - \frac{(kh)^2}{10} m_{pq}) E_x^p E_y^q \phi_{m,n} = 0} \tag{8.97}$$

These four stencils are associated with the following nodes where the range on the sum (p, q) is indicated.

$(\phi_{m,n})$	corner nodes	$(p,q) \in$	$\{-2,2\} \times \{-2,2\}$
$(\phi_{m+1,n})$	x-direction edge nodes	$(p,q) \in$	$\{0,2\} \times \{-2,2\}$
$(\phi_{m,n+1})$	y-direction edge nodes	$(p,q) \in$	$\{-2,2\} \times \{0,2\}$
$(\phi_{m+1,n+1})$	interior nodes	$(p,q) \in$	$\{0,2\} \times \{0,2\}$

Expressions for the difference coefficients $[s_{pq}]$ and $[m_{pq}]$ for consistent mass follow:

1. Corner Nodes

$$[s_{pq}] = \begin{bmatrix} 1 & -2 & -8 & -2 & 1 \\ -2 & 4 & 16 & 4 & -2 \\ -8 & 16 & 64 & 16 & -8 \\ -2 & 4 & 16 & 4 & -2 \\ 1 & -2 & -8 & -2 & 1 \end{bmatrix}; \quad [m_{pq}] = 2 \begin{bmatrix} -1 & 5 & -3 & 5 & -1 \\ 5 & -16 & -18 & -16 & 5 \\ -3 & -18 & 112 & -18 & -3 \\ 5 & -16 & -18 & -16 & 5 \\ -1 & 5 & -3 & 5 & -1 \end{bmatrix}$$

2. Side Nodes

$$[s_{pq}] = \begin{bmatrix} 5 & 0 & 5 \\ -16 & -48 & -16 \\ -18 & 176 & -18 \\ -16 & -48 & -16 \\ 5 & 0 & 5 \end{bmatrix}; \qquad [m_{pq}] = \begin{bmatrix} -1 & -8 & -1 \\ 2 & 16 & 2 \\ 8 & 64 & 8 \\ 2 & 16 & 2 \\ -1 & -8 & -1 \end{bmatrix}$$

3. Interior Nodes

$$[s_{pq}] = 8 \begin{bmatrix} -1 & -3 & -1 \\ -3 & 32 & -3 \\ -1 & -3 & -1 \end{bmatrix}; \qquad [m_{pq}] = \begin{bmatrix} 1 & 8 & 1 \\ 8 & 64 & 8 \\ 1 & 8 & 1 \end{bmatrix}$$

For the case of biquadratic elements, the numerical solutions are allowed to assume four different amplitudes corresponding to each of the four different stencils,

$$\begin{aligned} \phi_{m,n} &= A_1 \mu_x^m \mu_y^n \\ \phi_{m+1,n} &= A_2 \mu_x^{m+1} \mu_y^n \\ \phi_{m,n+1} &= A_3 \mu_x^m \mu_y^{n+1} \\ \phi_{m+1,n+1} &= A_4 \mu_x^{m+1} \mu_y^{n+1} \end{aligned} \tag{8.98}$$

where

$$\mu_x = \mathrm{e}^{ik_x^h \Delta x} \qquad \text{and} \qquad \mu_y = \mathrm{e}^{ik_y^h \Delta y} \tag{8.99}$$

The constants A_1 and A_4 represent amplitudes at the corner and the interior nodes of the element, while A_2 and A_3 denote the amplitudes at the edges parallel to the x and y axis respectively. Substituting the above discrete solutions into each recurrence stencil yields the characteristic matrix equations,

$$\boxed{[\tilde{\boldsymbol{S}} - \frac{(kh)^2}{10}\tilde{\boldsymbol{M}}]\boldsymbol{A} = 0} \tag{8.100}$$

where $\tilde{\boldsymbol{S}}$ and $\tilde{\boldsymbol{M}}$ are symmetric (4×4) characteristic matrices depending on $(k_x^h h)$ and $(k_y^h h)$, and $\boldsymbol{A} \in \mathbb{R}^4$ is the column of amplitudes. The characteristic functions $[\tilde{S}_{ij}]$ and $[\tilde{M}_{ij}]$ for consistent mass are as follows:

$$\begin{aligned}
\tilde{S}_{11} &= 56 - 2f_1 f_2 - 3f_1 - 3f_2 & \tilde{M}_{11} &= 16 - f_1 f_2 - 4f_1 - 4f_2 \\
\tilde{S}_{12} &= 10g_1 f_2 - 18g_1 & \tilde{M}_{12} &= -2g_1 f_2 + 8g_1 \\
\tilde{S}_{13} &= 10f_1 g_2 - 18g_2 & \tilde{M}_{13} &= -2f_1 g_2 + 8g_2 \\
\tilde{S}_{14} &= -32g_1 g_2 & \tilde{M}_{14} &= 4g_1 g_2 \\
\tilde{S}_{22} &= 88 & \tilde{M}_{22} &= 32 - 8f_2 \\
\tilde{S}_{23} &= -32g_1 g_2 & \tilde{M}_{23} &= 4g_1 g_2 \\
\tilde{S}_{24} &= -48g_2 & \tilde{M}_{24} &= 16g_2 \\
\tilde{S}_{33} &= 88 & \tilde{M}_{33} &= 32 - 8f_1 \\
\tilde{S}_{34} &= -48g_1 & \tilde{M}_{34} &= 16g_1 \\
\tilde{S}_{44} &= 128 & \tilde{M}_{44} &= 64
\end{aligned}$$

where

$$f_1 = \cos(k_x^h h) \qquad g_1 = \cos(k_x^h h/2)$$

$$f_2 = \cos(k_y^h h) \qquad g_2 = \cos(k_y^h h/2)$$

The dispersion relation is obtained by setting the determinant of this characteristic equation system to zero. For biquadratic elements, there are two frequency ranges (branches) where waves are allowed to propagate with pure real wavenumbers. Figure 8.20 shows surface plots of the relative phase speed $c^h/c = k/k^h$ as a function of the normalized wavenumber components $0 < k_x^h h/\pi < 1$ and $0 < k_y^h h/\pi < 1$ corresponding to the lower branch surface. For propagation along mesh lines $\theta = 0$

mod 90, these two-dimensional dispersion relations reduce to the one-dimensional relations derived in THOMPSON AND PINSKY [1993b]. Comparing these results to the dispersion surfaces for bilinear elements, it is clear that biquadratic discretizations exhibit less phase error for the same number of nodes per wavelength.

8.9.4 Optimal GLS parameter for quadratic elements

For a nonzero GLS parameter $\tau \neq 0$, additional equations are added to the Galerkin equations as prescribed by (8.34). The optimal definition of τ_{quad} using quadratic $p = 2$ basis functions for plane-waves propagating along mesh lines, has been reported in THOMPSON AND PINSKY [1993c,1993d]. With this assumption, the problem reduces to one-dimension and the Laplacian operator is interpreted as $\nabla^2\phi = \phi,_{xx}$. Application of the discrete Fourier transform to these equations, and requiring that the phase be exact in the x-direction, $k_x^h = k$, leads to the definition of τ_{quad}. By substituting the exact wave number into the finite element dispersion relation for quadratic elements, a quadratic equation for the optimal value of τ is obtained. Defining the nondimensional parameters $\alpha := kh$, and $\hat{\tau} := \tau k^2$, this equation is given by,

$$c_2\hat{\tau}^2 + c_1\hat{\tau} + c_0 = 0 \tag{8.101}$$

where

$$\begin{aligned}
c_0(\alpha) &= -240(1-\cos\alpha)\alpha^2 + 8(13+2\cos\alpha)\alpha^4 + (-3+\cos\alpha)\alpha^6 \\
c_1(\alpha) &= -2880(1-\cos\alpha) + 1440\alpha^2 + 24(-6+\cos\alpha)\alpha^4 + 2(3-\cos\alpha)\alpha^6 \\
c_2(\alpha) &= -240(1-\cos\alpha)\alpha^2 + 40(1-\cos\alpha)\alpha^4 + (-3+\cos\alpha)\alpha^6
\end{aligned}$$

The optimal GLS parameter τ_{quad} is obtained by solving this quadratic equation, i.e.

$$\boxed{\tau k^2 = \frac{-c_1 \pm \sqrt{c_1^2 - 4c_0c_2}}{2c_2}} \tag{8.102}$$

For quadratic elements, there are two frequency ranges where waves are allowed to propagate with real wavenumbers. In the above expression, the minus sign is used

Figure 8.20: Surface plot of phase error $e_p = (c^h/c)$ vs. normalized wave vector components $(k_x^h h/\pi)$ and $(k_y^h h/\pi)$ for biquadratic elements with $\tau = 0$: (a) exact integration (b) diagonal mass matrix (lobatto quadrature)

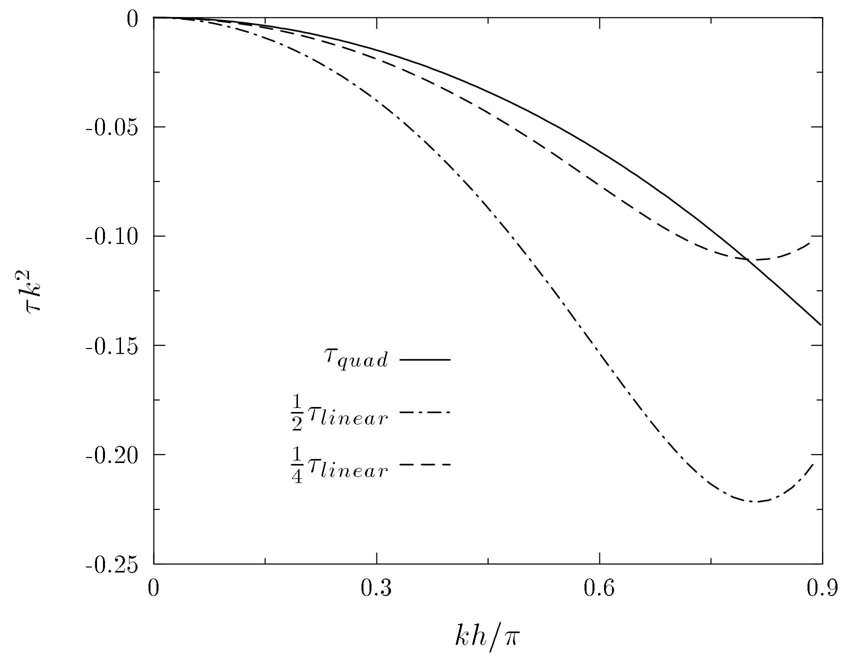

Figure 8.21: GLS mesh parameter τ_{quad} for quadratic interpolation compared to estimates based on fractions of the linear τ_{linear}.

for the range $0 < kh < \pi$ while a plus sign is used for the range $\pi < kh < 2\pi$, where 2π is the limit of resolution for quadratic elements. At $kh = \pi$, there exists a discontinuity in the value of τ_{quad}. This phenomena is related to the so-called 'stopping bands' present in high-order finite element discretizations where allowed waves possess amplitude attenuation; further discussions related to this phenomena are given in the complex wavenumber analysis performed in the next Chapter. Figure 8.21 plots τ_{quad} together with simple approximations based on fractions of the GLS parameter derived earlier for linear interpolations in the operating range of two elements per wavelength or greater. A practical estimate, useful for computation is $0.25\tau_{linear}$.

8.10 Summary and Conclusions

In this Chapter we have presented a Galerkin/Least-Squares (GLS) finite element method for multi-dimensional wave propagation governed by the Helmholtz equation. The GLS parameter τ is designed from the criterion that numerical phase error be reduced in the primary direction of wave propagation. Results from a multi-dimensional discrete Fourier analysis of the GLS method indicate that the additional least-squares operator improves the accuracy of the Galerkin solution over all wave vector orientations. Accurate GLS solutions are maintained for as little as six linear elements per wavelength compared to the limit of ten elements per wavelength required for well resolved Galerkin solutions.

A number of alternative GLS parameters were derived for general numerical integration rules such as Gaussian and Lobatto quadrature. Results from the dispersion analysis indicate that phase accuracy and directional properties associated with GLS using either exact integration, or diagonal mass approximations, are significantly improved when compared to Galerkin.

Numerical examples of plane waves traveling along a two-dimensional waveguide with uniform, rotated, and distorted mesh orientations verify that as the wavenumber, normalized with respect to the element size, is increased, the degradation in phase accuracy present in the Galerkin solution is reduced and in some cases eliminated by the proper choice of the GLS parameter τ. GLS solutions for the Green's function in the interior of simple rectangular domains demonstrates the improved performance compared to the standard Galerkin method where multiple reflections are present. These results validate our conclusion that for problems where waves are directed in arbitrary directions, use of the GLS parameter $\tau_{22.5}$ defined in (8.71) with $\theta_o = 22.5$, is more accurate than the use of τ_0, designed to give exact phase for one-dimensional solutions.

By increasing the circumferential harmonics for a radiating cylindrical model, the response of individual modes on the performance of the numerical solutions has been investigated. Results indicate that for low modes, the radiated energy of the cylindrical waves are best resolved by the GLS parameter τ_0, designed to improve dispersion errors for plane-waves directed along the radial rays, while for higher modes, the alternate GLS parameter $\tau_{22.5}$, designed for arbitrary directional wave vectors performs optimally.

Optimal GLS parameters for the Helmholtz equation in $\mathbb{R}^3$ are also reported. Detailed derivations and dispersive properties for trilinear finite element discretizations will be published in a subsequent manuscript. The extension to a Generalized Galerkin/Least-Squares (GGLS) method has also been investigated; dispersion results show that for bilinear elements on a uniform grid, the phase accuracy for GGLS is the same as GLS over all wave vector orientations. The dispersion properties of biquadratic finite element discretizations has also been examined. Results show that for well resolved waves, biquadratic elements exhibit significantly less phase error compared to bilinear elements for the same number of nodes per wavelength. The extension of the GLS method to higher-order interpolations has also been indicated. The optimum GLS mesh parameter for quadratic elements is given. GLS finite elements for time-harmonic wave propagation using higher-order basis functions require that a suitable definition of τ be obtained for each spectral order p. In this work, it was shown that GLS parameters for elements with basis functions of high spectral order p can be approximated by simple fractions of low-order GLS parameters. In particular, for quadratic elements ($p = 2$), the value $\tau = .25\tau_{linear}$ proves to be a useful estimate.